Lithologies and Chronologic Opportunities of Materials to be Returned from the Artemis Exploration Zone

Ruby V. Patterson[1], Thomas J. Lapen[1], David A. Kring[2], Myriam Lemelin[3], and McKayla L. Meier[4]

[1*]University of Houston.[2]Lunar and Planetary Institute.[3]Université de Sherbrooke.[4]University of Florida.

Corresponding author: Ruby Patterson (rubypatterson1@gmail.com)

*Alternate affiliation: Jacobs at NASA Johnson Space Center, 2101 NASA Parkway, Building 31, Room 156, Houston, TX, 77058; ruby.v.patterson@nasa.gov.

Key Points:

- The Artemis lunar missions will explore a feldspathic impact terrain and return samples from unexplored terrain.
- Likely lithologies, ages, and chronometers are discussed for six potential landing sites.
- Artemis return samples from will be unique from Apollo samples and have the possibility of determining absolute ages of significant events in lunar history.

Abstract

The Artemis exploration zone is a geologically-complex region likely hosting some of the oldest and as-yet-unstudied materials on the Moon. We review six potential Artemis landing sites (001, 004, 007, 011, 102, and 105) within candidate Artemis III landing regions 'Connecting Ridge,' 'Peak Near Shackleton,' 'Leibnitz Beta Plateau,' 'de Gerlache Rim,' and 'de Gerlache Rim 2.' Kaguya Spectral Profiler mineral data were used to determine average lithological composition at each landing site. Potentially accessible geologic materials, their ages and significance, and appropriate application of radiometric chronometers are discussed in reference to return samples from each potential landing site. Chronologic analyses of return samples from the Artemis exploration zone will enable the anchoring of the lunar impact flux curve, determine the absolute timing of pivotal events in lunar geologic history, and reveal geological diversity of the differentiated lunar body.

Plain Language Summary

Artemis astronauts will bring new samples from the Moon back to Earth. We discuss the geology of some landing sites the astronauts might visit, what types of rocks they may encounter, and how to examine them using geochronology. The application of geochronology to Moon rocks is essential to know the absolute timing of major events in lunar and early Solar system history.

1 Introduction

The Artemis exploration zone (AEZ) includes terrain dominated by photogeologically-mapped and stratigraphically-determined Nectarian and pre-Nectarian age surfaces. These surfaces have materials that can help answer important questions regarding impact chronology, history of major lunar events such as formation and differentiation, and an opportunity to sample deeply excavated materials. To answer these questions, detailed petrologic analyses coupled with chronologic analyses of specimens collected from the AEZ are required.

Examination of impact-cratered surfaces can determine fluxes in impact events in lunar history (Neukum et al., 1975; Boyce et al., 1977; Kring, 2008; Mazrouei et al., 2019; Lagain et al., 2022; Fairweather et al., 2022). Establishing the ages of specific impact craters and basins is important because these ages can anchor a crater chronology of the lunar surface (Arvidson et al., 1979; Neukum, 1984; Neukum et al., 2001; Che et al., 2021; Yue et al., 2022) and better define the bombardment history of the inner solar system (Kring et al., 2005; Kring, 2006, 2007, 2008, 2009). The returned lunar samples by the Apollo program were subjected to radioisotope dating, but many of the sampling sites might be part of the perturbated megaregolith formed by ejecta of large impact basins (Howard et al., 1974; Moore et al., 1974; Head et al., 1993; Haskin, 1998; Haskin et al., 1998; Petro and Pieters, 2008) and many studied specimens cannot be reliably attributed to a specific impact event (Korotev et al., 2002). The Imbrium basin is dated at roughly ~3.5 Ga (Deutsch and Stöffler, 1987; Spudis et al., 1988; Merle et al., 2014; Zhang et al., 2015), but ages of other significant lunar basins, such as the Orientale Basin, have yet to be firmly established (Stöffler et al., 2006; Meyer et al., 2016; Wu et al., 2019). The mapped ages of features in Figure 1 are in flux based on crater-counting ages determined from orbit (Tye et al., 2015; Deutsch et al., 2020). While Spudis et al. (2008) mapped Shackleton crater with a 3.6 Ga age, Zuber et al. (2012), Tye et al. (2015), and Kring et al. (2021) reported Imbrian ages of ~3.69 Ga, 3.51 +0.05/-0.08 Ga,

and 3.43 +0.04/-0.05 Ga, respectively. Moreover, while Spudis et al. (2008) mapped Shoemaker and Faustini craters with Nectarian ages, Tye et al. (2015) report pre-Nectarian ages, similar to those at Haworth. The variable age estimates illustrate the need for sample return and radiometric analyses in Earth-based laboratories. The age of the South Pole-Aitkin (SPA) basin, thought to be the oldest and largest basin on the Moon and, thus, a key anchor point in defining the lunar chronology, is still not precisely known (Wilhelms et al., 1987; Hiesinger et al., 2012). The South Pole-Aitken Terrane has not yet been directly sampled but it is the focus for the crewed Artemis missions (Jolliff et al., 2000) (Figure 1).

Sampling impact-generated pre-Nectarian- and Nectarian-age materials in the Artemis exploration zone also provides a way to test the crater counting calibration curve and refine the impact flux during the first billion years of Earth-Moon history; i.e., testing the lunar cataclysm

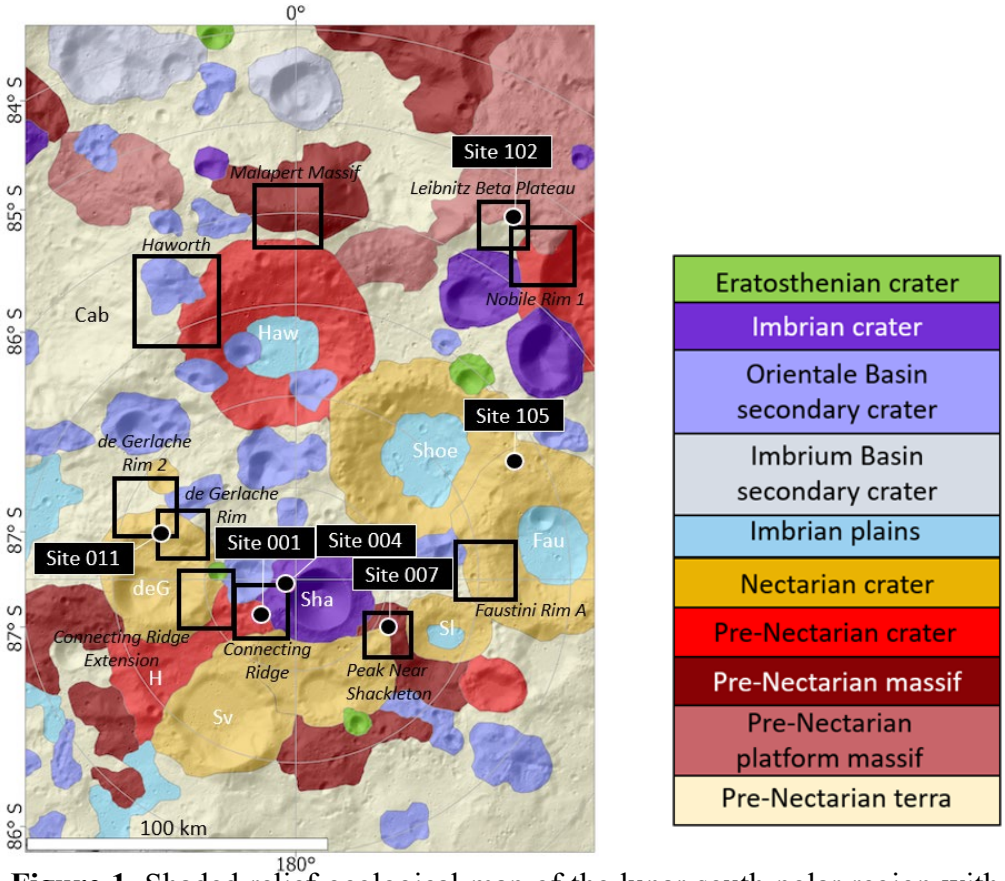

Figure 1. Shaded relief geological map of the lunar south polar region with the locations of several potential Artemis landing sites (001, 004, 007, 011, 102, and 105). Base map by Allender et al. (2019) in the LPI Lunar South Pole Atlas using geology of Spudis et al. (2008) and Lunar Orbiter Laser Altimeter data. The mapped ages of features are in flux based on crater-counting ages determined from orbit. For example, while Spudis et al. (2008) mapped Shackleton crater with a 3.6 Ga age, Zuber et al. (2012), Tye et al. (2015), and Kring et al. (2021) reported Imbrian ages of ~3.69 Ga, 3.51 +0.05/-0.08 Ga, and 3.43 +0.04/-0.05 Ga, respectively. Moreover, while Spudis et al. (2008) mapped Shoemaker and Faustini craters with Nectarian ages, Tye et al. (2015) report pre-Nectarian ages, similar those that of Haworth. Those disparate ages illustrate the need for sample return and radiometric analyses in Earth-based laboratories. Cab- Cabeus; Haw- Haworth; Shoe- Shoemaker; Fau- Faustini; deG- de Gerlache; Sha- Shackleton; Sl- Slater; H- Henson; Sv- Sverdrup.

hypothesis, which is the highest priority science objective as defined by the National Research Council (NRC) (2007). In addition, the region may contain debris from the SPA basin. Recovering debris with an SPA impact-reset age will provide an opportunity to address the second highest priority science objective (NRC, 2007): to provide an anchor to the basin-forming epoch on the Moon. Currently, ages for SPA range from 4.39 Ga to 4.25 Ga (Hiesinger et al., 2012; Morbidelli et al., 2012). Collectively, those data will refine the crater calibration curve, which can then be applied to surfaces around the entire Moon and other planetary surfaces in the Solar system. The

pre-Nectarian and Nectarian impact events in the Artemis exploration zone excavated and produced breccias composed, in part, of unusually old highland terrain crust. Samples of that material could provide additional opportunities to constrain the timing of the giant Moon-forming impact, lunar differentiation, crustal formation, and subsequent magmatism, which are tied to several other important scientific objectives (NRC, 2007; Artemis III Science Definition Team Report).

The impact cratering process is critical for excavating materials from depth and allows access to materials that may otherwise be deeply buried. Exhumed lithologies also provide information on the local stratigraphy (Pieters et al., 1994; Kring, 2009; Kenkmann and Artemieva, 2021), for example, at Shackleton crater (Gawronska et al., 2020). Because SPA is the largest and oldest impact basin on the Moon (Wilhelms et al., 1987), it may contain rare upper mantle materials at the surface in select locations (Moriarty et al., 2021). Thus, a cross-section of lunar crust up to 10's of kilometers deep may be developed if the return sample collection strategy includes samples collected from varied crater features (e.g., modification zones, central uplifts, etc.) and impact breccias (Kring, 2009). Impact crater ejecta may also allow for the determination of the average composition of impacted crust from the sampling of homogenized subsurface lithologies in the form of impact melt materials (Kring, 2009). The environmental consequences (e.g., dust lofting, ejecta blanketing, flood basalts, rockfall; mountain-forming, etc.) of these impacts may also be inferred through orbital, field, and sample observation of impact craters (Mukhametshin et al., 2018; Michaut and Pinel, 2018; Xie et al., 2020; Bickel et al., 2020). The delivery and abundance of elements through impacts may also be determined and used to piece together a history of the chemical evolution of the lunar interior and crust (Bottke et al., 2010; Barnes et al., 2016; Joy et al., 2016, 2020; Zhu et al., 2019). Finally, investigations and sampling of heavily impact-cratered terrain may also provide access to impact melt samples from other craters (Kring et al., 2005; Kring, 2007, 2009).

This study reviews six potential Artemis landing sites (001, 004, 007, 011, 102, and 105) within candidate Artemis III landing regions 'Connecting Ridge,' 'Peak Near Shackleton,' 'Leibnitz Beta Plateau,' 'de Gerlache Rim,' and 'de Gerlache Rim 2' (NASA, 2020b, 2022). The numbered potential landing sites correspond to the illumination sites identified in previous work (Bussey et al., 2010; Mazarico et al., 2011; Speyerer and Robinson, 2013). Kaguya Spectral Profiler mineral count data were used to determine average lithological composition at each landing site. Potential accessible geologic materials, their ages and significance, and appropriate application of radiometric chronometers are discussed in reference to return samples from each potential landing site. Chronologic analyses of return samples from the Artemis exploration zone will enable the anchoring of the lunar impact flux curve, determine the absolute timing of pivotal events in lunar geologic history, and reveal geological diversity of the differentiated lunar body.

1.1 Input Data

Kayuga Spectral Profiler (SP) is a visible to near infrared spectrometer with a ~500 m spatial footprint acquiring data via three spectral bands (one visible, two near infrared) between 500 and 2600 nm (Haruyama et al., 2008). However, topography in the polar regions causes different surfaces to receive widely uneven solar illumination, from no direct incident sunlight in topographic depressions (such as permanently shaded regions) to abundant sunlight on steep Sun-facing slopes, which makes spectral interpretation challenging. Lemelin et al. (2022) converted

the SP radiance data (level 2B1) measured in each SP orbit into bidirectional reflectance using the photometric function of Yokota et al. (2011), which allowed the conversion of radiance data into reflectance data at a standard viewing geometry of 30° incidence angle and 0° emission angle. However, as the photometric function of Yokota et al. (2011) assumes a flat sphere, reflectance measurements higher or lower than expected occur on sloped surfaces. The Lunar Orbiter Laser Altimeter (LOLA) onboard LRO acquires reflectance data at 1064 nm and is unaffected by slope effects as it sends its own illumination. Lemelin et al. (2022) thus scaled the gridded SP reflectance data to the gridded and calibrated LOLA data at their common wavelength of 1064 nm. They could then calculate FeO abundances using reflectance data at 750 and 950 nm, and use Hapke radiative model (e.g., Hapke, 1981, 2001) to estimate the abundance of olivine, low-calcium pyroxene (LCP), high-calcium pyroxene (HCP), and plagioclase on continuum removed spectra, using FeO

	Potential Landing Site					
	001	004	007	011	102	105
Copernican < 0.80 Ga						
Eratosthenian 0.8 to 3.20 Ga						
Upper Imbrian 3.20 to 3.80 Ga	Shackleton	Shackleton				
Lower Imbrian 3.80 to 3.85 Ga	Shackleton Spudis, Marvin, Orientale (Secondary)	Shackleton Spudis + Orientale (Secondary)		Orientale (Secondary)		Malinkin + Orientale (Secondary)
Nectarian 3.85 to 3.92 Ga	de Gerlache, Unnamed?			de Gerlache		Shoemaker + Faustini
pre-Nectarian > 3.92 Ga	Henson, Sverdrup, Marvin	Sverdrup	Slater Massif Terra	Terra	Nobile Platform Massif Terra	Terra

Figure 2. Summary of age units at each potential landing site in accordance with Figure 1. Upper and lower age limits of each time period are from Stöffler et al. (2006). Although not visible at the scale mapped in Figure 1, all sites will contain small Copernican-age craters.

as a constraint. We used these gridded mineral maps and the gridded abundance of FeO to study the probable geology of the Artemis region.

1.2 Potential Landing Sites

The Artemis III mission will not be supported with a rover, so crew will be limited to walking extravehicular activities (EVAs) within 2 km distance of the Human Landing System (HLS) (Coan, 2020; Kring et al., 2023). An unpressurized Lunar Terrain Vehicle (LTV) will be deployed

for later missions (NASA, 2021, 2023) and should provide an exploration range up to 10 km radial distance from a lander. For the purposes of our study, we utilize that 10 km radial distance around potential Artemis landing sites to evaluate the types of samples available for collection and return to Earth.

1.2.1 Site 001 (‘Connecting Ridge’ region)

Potential Artemis landing site 001 (NASA, 2020a) (Site “SP-1” at (-89.45, 222.69) in Mazarico et al. (2011); “Point B” at (89.44°S, 141.8°W) in Bussey et al. (2010)) is within the Artemis III candidate landing region called “Connecting Ridge” and located on a massif ridge connecting Shackleton and Henson craters (Figure 1a). This ridge itself is roughly pre-Nectarian in age (Stöffler et al., 2006) but is cross-cut by Shackleton crater and secondary crater ejecta believed to be of significantly younger Imbrian age (3.51 to 3.69 ± 0.4 Ga) (Spudis et al., 2008; Zuber et al., 2012). The ridge will be covered with Shackleton ejecta, potentially including fragments of the original highland crust, components from the lunar magma ocean and later intrusive rocks, cryptomare from SPA, plus impact melts from Shackleton, SPA, and other pre-Nectarian impacts (Kring, 2019; Halim et al., 2021; Kring et al., 2022). Anticipated dominant lithologies are anorthosite below the Shackleton crater rim down to ~900 m, regolith, and breccia (Gawronska et al., 2020). Lowest FeO values within the Artemis exploration region determined by Kaguya SP (~5 to 7 wt. %) are found in the 89° to 90°S region near Shackleton crater (applies to Site 004 as well) (Lemelin et al., 2022).

1.2.2 Site 004 (along margin of ‘Connecting Ridge’ region)

Potential Artemis landing site 004 (NASA, 2020a) (Site “SP-4” at (-89.78, 204.27) in Mazarico et al. (2011); “Point A” at (89.68°S, 166.0°W) in Bussey et al. (2010)) is along the margin of Artemis III candidate landing region called “Connecting Ridge” on a portion of Shackleton crater (ridge is pre-Nectarian age, 4.52 to 3.92 Ga, (Stöffler et al., 2006); crater is Imbrian age; 3.6 ± 0.4 Ga (Spudis et al., 2008; Zuber et al., 2012; Tye et al., 2015; Halim et al., 2021)) rim and is nearly coincident with the geographic south pole of the Moon (Figure 1). Imbrium secondary crater materials and pre-Nectarian ejecta from Henson crater are accessible within a 10 km radial distance (Figure 2). This site contains multiple rock exposures (Gawronska et al., 2020). Anticipated lithologies include pure anorthosite exposures (Yamamoto et al., 2012; Lemelin et al., 2017). Sites 001 and 004 provide a unique opportunity to sample rays from Tycho crater that reach directly between the two sites (Lemelin et al., 2022). Both sites provide an opportunity to sample pre-Nectarian crater, Imbrian crater, and Imbrian secondary crater materials.

1.2.3 Site 007 (‘Peak near Shackleton’ region)

Potential Artemis landing site 007 (NASA, 2020a) (Site “SP-7” at (-88.81, 123.64) in Mazarico et al. (2011); “Point D” at (88.79°S, 124.5°E) in Bussey et al. (2010)) is within the Artemis III candidate landing region “Peak near Shackleton” located on a massif ridge between Shackleton and Slater craters (Figure 1a). Within a 10 km radial distance, Site 007 would enable the sampling of materials from the pre-Nectarian massif, Nectarian crater, and Imbrian crater (Figure 2). This site may provide the possibility to observe layered strata from Shackleton and compare ejecta and stratigraphy with Slater crater. Layered terrain is 10 to 50 m thick in Shackleton (Halim et al., 2021). The lateral extent of these layers is difficult to observe due to poor illumination conditions, but they may be ejecta produced from older impacts (i.e., Haworth, Shoemaker, Faustini).

Interestingly, numerical modeling efforts have determined the top bed in this stratigraphic sequence may contain over ~150 m of Shackleton ejecta (Halim et al., 2021). Kumari et al. (2022) identified 3,204 resolvable boulders (ranging from 0.7 to 14 m diameter) within a 10 km radius of site 007.

1.2.4 Site 011 (‘de Gerlache Rim 1’ and ‘de Gerlache Rim 2’ regions)

Potential Artemis landing site 011 (NASA, 2020a) (Site “SP-11” at (-88.67, 291.90) in Mazarico et al. (2011); “Point C” at (88.71°S, 68.7°W) in Bussey et al. (2010)) is within the Artemis III candidate landing region “de Gerlache Rim”. De Gerlache Rim 1 is approximately centered on the crater rim, while de Gerlache Rim 2 is mostly north of the crater rim (Figure 1). Based on absolute crater counting models, de Gerlache is believed to be Nectarian in age (Tye et al., 2015; Deutsch et al., 2020) and, just beyond de Gerlache Rim 1, its rim is cross-cut by an Eratosthenian-age Marvin crater. The de Gerlache impact appears to be younger than the pre-Nectarian ‘Connecting Ridge’ massif (Spudis et al., 2008) and, thus, may have covered the massif with ejecta prior to the Shackleton impact. Pre-Nectarian terra, Nectarian crater, and Imbrian secondary crater materials are present within a 10 km radial distance from Site 011 (Figure 2). This site may allow for volatile sampling within secondary craters and comparison to Apollo permanently shadowed region (PSR) crater samples (Li and Milliken, 2017; Kereszturi et al., 2022). The de Gerlache ejecta within the region may provide samples of anorthositic crustal lithologies and SPA ejecta. Within a 10 km radial distance around site 011, over 3,774 boulders from 0.7 to 26 m in diameter have been identified (Kumari et al., 2022).

1.2.5 Site 102 (‘Leibnitz Beta Plateau’ region)

Potential Artemis landing site 102 (NASA, 2020a) (Site “SP-20” at (-85.43, 31.73) in Mazarico et al. (2011)) is within the Artemis III candidate landing region called “Leibnitz Beta Plateau” located atop informally-named Mons Leibnitz Beta, which is now called Mons Mouton (Figure 1). The Leibnitz Mountains lie on the topographically-high ring outlining the SPA basin (Garrick-Bethell and Zuber, 2009). This plateau is bounded by a nearly vertical cliff facing south-poleward. The cliff may provide a unique opportunity to access a roughly 8-km-thick cross-section of lunar crust. Massifs like Mons Mouton may also provide an opportunity to identify additional lithologies produced by early lunar magmatic processes. This site may allow for sampling from adjacent pre-Nectarian and Nectarian aged impacts Haworth (4.18 ± 0.02 Ga), Shoemaker (4.15 ± 0.02 Ga), and Faustini (4.10 ± 0.03 Ga) craters (Figure 2; Tye et al., 2015). NASA’s VIPER rover is set to

land and traverse near this site to search for and sample volatiles up to approximately 1 meter deep within the regolith (Shirley and Balaban, 2022).

1.2.6 Site 105

Potential Artemis landing site 105 (NASA, 2020a) ((-87.18, 62.84) in Patterson et al. (2022) is located between pre-Nectarian aged Shoemaker (4.15 ± 0.02 Ga) and Faustini (4.10 ± 0.03 Ga) craters (Tye et al., 2015) (Figures 1, 2). Site 105 is downslope from Site 102. This region contains many large blocks and boulders (1.5 to 9 m diameter) (Patterson et al., 2022) and the floors of Shoemaker and Faustini likely house icy volatile deposits (Tye et al., 2015; Patterson et al., 2022; Brown et al., 2022), and the ridge bisecting Faustini and Shoemaker crater rims has ejecta deposits likely to be up to Nectarian in age (Tai Udovicic et al., 2022). This site contains the lowest FeO values (~5-7 wt. %) of all of the 84° to 90° S region (Figure 1a; Lemelin et al., 2022).

Table 1. Commonly applied radiogenic isotope systems and the methods by which they may be analyzed.

Isotope System	**Analytical Technique**				
	Bulk sample or glass	Mineral/ bulk rock isochron	Single mineral	In-situ (Laser ablation/ secondary ion)	Wet chemistry
$^{40}K \rightarrow {}^{40}Ar$ (^{40}Ar - ^{39}Ar)	X		X	X	
$^{87}Rb \rightarrow {}^{87}Sr$		X		X	X
$^{147}Sm \rightarrow {}^{143}Nd$		X			
$^{146*}Sm \rightarrow {}^{142}Nd$		X			
$^{176}Lu \rightarrow {}^{176}Hf$		X	X	X	X
$^{187}Re \rightarrow {}^{187}Os$		X			
$^{232}Th \rightarrow {}^{208}Pb$		X	X	X	X
$^{235}U \rightarrow {}^{207}Pb$		X	X	X	X
$^{238}U \rightarrow {}^{206}Pb$		X	X	X	X

2 Isotope Chronology

The timing of major events, including the timing of lunar differentiation, duration of igneous activity, and impact history, can be constrained with isotope chronology of lunar materials (e.g., Nyquist and Shih, 1992). Foundational chronologic analyses of Apollo 11 samples are summarized in the Proceedings of the Apollo 11 Lunar Science Conference (1970) and "The Moon Issue" of the journal Science (Abelson, 1970, and articles in the issue) and laid the groundwork for all future studies of lunar return samples. The commonly applied isotope systems are summarized in Table 1 and described below. Each radiometric system is best suited to a particular subset of geologic events and temperatures. For example, some approaches are best suited to date high-temperature igneous crystallization, whereas other systems best reflect cooling below 300 to 500 ºC. Furthermore, the radiometric systems may require specific minerals and/or chemical compositions. Thus, some chronologic approaches may be more suitable to different lunar lithologies than others, simply by the nature of the texture and/or mineralogy of the sample. The

ages of secondary processes, such as impact metamorphism, may also be determined, depending on the material and degree of metamorphism/melting.

2.1 U-Th-Pb

The ^{238}U-^{206}Pb, ^{235}U-^{207}Pb, and ^{232}Th-^{208}Pb isotope systems are some of the most versatile isotope systems that can be applied to a wide variety of lunar lithologies. These systems were developed prior to the Apollo 11 mission and were applied to the first returned specimens (e.g., Silver, 1970; Tatsumoto and Rosholt, 1970). Because ^{238}U-^{206}Pb and ^{235}U-^{207}Pb reflect two isotope systems in the U-Pb system, ages can be determined using multiple approaches including standard U-Pb isochrons, inverse Pb-Pb isochrons, and U-Pb concordia diagrams (e.g., Wetherill and Tera-Wasserburg diagrams). The ^{238}U, ^{235}U, and ^{232}Th half-lives are 4.468, 0.704, and 14.01 Ga, respectively (Steiger and Jäger, 1977). Despite recent studies that refine the decay constants (e.g., Amelin and Zaitsev, 2002; Schoene et al., 2006), the IUGS-IUPAC recommends the decay constants of Jaffey et al. (1971) for ^{238}U and ^{235}U (Villa et al., 2022). Uranium and Th-rich and high U/Pb and/or Th/Pb ratio trace phases such as zircon, baddeleyite, zirconolite, tranquillityite, apatite, merrillite, and monazite are documented in many lunar lithologies and have the potential for precise chronology (e.g., Lovering et al., 1974; Rasmussen et al., 2008; Barboni et al., 2017; Shaulis et al., 2017). Even in materials without these trace phases, many lunar rocks and/or their sources have relatively high ^{238}U/^{204}Pb ratios (denoted as μ) of about 360 to over 2600 for lunar basaltic rocks (e.g., Snape et al., 2018) whereas the μ-value of the terrestrial mantle is about 8 (e.g., Ballhaus et al., 2013).

Since most lunar rocks have experienced secondary processes such as thermal and/or impact metamorphism, some mineral hosts are more resilient to disturbances of the U-Th-Pb systems than others. For example, zircon has the potential to preserve the U-Th-Pb systematics of crystallization from a melt and will retain those characteristics even through metamorphic events that would disturb U-Th-Pb in other materials (Cherniak and Watson, 2001). Zircon is considered one of the most robust time capsules nature has to offer. Uranium and Pb in baddeleyite also has the potential to record igneous events despite the host rock being subjected to high-grade metamorphic conditions (Niihara et al., 2009). Microstructural analyses of trace phases such as baddeleyite can reveal relict polymorphs that provide additional context for age data (White et al., 2020). Other U and/or Th-rich mineral hosts such as apatite, however, are less resistant to disturbances than zircon for any given temperature-time (T-t) history (Chew et al., 2021) and can record the timing of metamorphic events (Nemchin et al., 2009).

Analytical approaches for U-Th-Pb analyses include in-situ (minimally destructive) or wet chemical (fully destructive). In-situ analyses usually involve either a laser or secondary ion source that samples the material of interest at spatial resolutions between 5 and 100 μm. The advantages of in-situ approaches are that analyses often have petrological context through microstructural and/or mineral textural data. Age data can be collected from very small specimens (Che et al., 2021) and clasts (Snape et al., 2018). One disadvantage of in-situ analyses is that the measurement precision is often significantly less than that of wet chemical approaches such as isotope-dilution thermal ionization mass spectrometry (ID TIMS; see Schoene (2014) for a full treatment of the methods). In lithologies that do not typically contain U and Th-rich trace phases, measurement of the ^{207}Pb/^{206}Pb and ^{204}Pb/^{206}Pb ratios of other phases such as pyroxene can yield precise ages. For example, Borg et al. (2011) measured an age of 4359.2 ± 2.4 Ma for sequentially-dissolved

pyroxene in ferroan anorthosite 60025. Overall, with modern analytical techniques, the ages of most lunar lithologies can be precisely determined with the U-Th-Pb systems.

2.2 Rb-Sr

The Rb-Sr isotope system has been applied to Apollo lunar materials since they were collected (Gopalan et al., 1970; Hurley and Pinson, Jr., 1970; Papanastassiou et al., 1970) and has the potential for precise chronology (Rankenburg et al., 2007) and chemical/isotopic tracing (Borg et al., 2022). The IUGS-IUPAC-recommended decay constant for ^{87}Rb is (1.3972 ± 0.0045) × $10^{-11}a^{-1}$ (Villa et al., 2015). Great care must be taken in comparing data because many studies used and/or still use the value of 1.42 × $10^{-11}a^{-1}$ reported in Steiger and Jäger (1977) and other studies may adopt the new decay constants. In any case, most published age data can be recalculated to the same or updated decay constant.

Strontium isotopic and ^{87}Rb/^{86}Sr ratios of rock, glass, and/or mineral materials are typically measured with wet chemical approaches (destructive analyses) where the materials are digested and Rb and Sr are chemically purified and analyzed (Charlier et al., 2006). Common lunar rock-forming minerals such as pyroxene, plagioclase, K-feldspar, and olivine have highly variable Rb/Sr ratios making them amenable for dating using the isochron approach. Very recent advancements in mass spectrometry have enabled in-situ analysis of ^{87}Sr/^{86}Sr and ^{87}Rb/^{86}Sr by laser ablation plasma-source mass spectrometry (Dauphas et al., 2022) opening a vast new area for investigation with a minimally-destructive, high-spatial resolution (~100 μm) technique.

In addition to chronology, the Rb-Sr system can be used as an isotope tracer. For example, Borg et al. (2022) model the Rb-Sr isotope systematics of the Earth, Moon, and Theia (the proto-Earth impactor) to constrain the timing of volatile addition and the timing of the Moon-forming event. The Rb-Sr isotope system can also be used to trace potential mixing relationships and the sources of lunar igneous rocks (Hui et al., 2013), and potentially define model age constraints in materials that cannot otherwise be dated (McLeod et al., 2016).

2.3 Sm-Nd

Similar to U-Pb, Sm-Nd consists of two isotope systems (^{146}Sm-^{142}Nd and ^{147}Sm-^{143}Nd) in one element system, except ^{146}Sm is now extinct. The Sm-Nd system has been applied to most lunar lithologies for chronology and tracers of magma sources (Nyquist et al., 1995; Brandon et al., 2009; Carlson et al., 2014; Borg et al., 2015; Johnston et al., 2022). The IUGS-IUPAC recommended half-lives of ^{146}Sm and ^{147}Sm are 0.068 – 0.103 and 106.25 ± 0.38 Ga, respectively (Villa et al., 2020). Given the uncertainty of the ^{146}Sm decay rate, recent papers (McLeod et al., 2014) use both half-life values of 0.068 and 0.103 Ga in their model calculations.

High-precision analyses of Sm-Nd requires wet chemical approaches and relatively large samples with minimum mass requirements of 0.05 to 1 g, depending on Sm and Nd concentrations, mineralogy, and grain size. Most lunar rocks and minerals have overall low concentrations of Sm and Nd (ppb to ppm concentrations) and limited natural variations in Sm/Nd ratios due to their similar geochemical characteristics in most materials. The range in ^{147}Sm/^{144}Nd ratios in most lunar minerals (feldspar, pyroxene, olivine, phosphate) is limited between about 0.14 to 0.30, unlike Rb-Sr, U-Th-Pb, and Lu-Hf where the range in parent/daughter ratios can be orders of magnitude greater. Despite the limited range in Sm/Nd ratios and resulting limited variations in

radiogenic Nd isotopic compositions, advancements in mass spectrometry allow very high precision (few ppm) measurements of $^{143}Nd/^{144}Nd$ and $^{142}Nd/^{144}Nd$ ratios (Rankenburg et al., 2006; Boyet and Carlson, 2007). These high-precision measurements are also required to accurately measure and ultimately correct neutron capture effects from cosmic ray exposure that can alter the Sm and Nd isotopic compositions (Nyquist et al., 1995; Brandon et al., 2009).

Measured Sm and Nd isotopic compositions corrected for neutron capture effects have yielded many robust ages of lunar materials (Carlson et al., 2014; Borg and Carlson, 2023). As opposed to the other isotope systems listed in Table 1, Sm and Nd are geochemically similar lanthanide elements that are relatively immobile during periods of shock metamorphism. Other elements, such as the alkalis (Rb), can be more easily mobilized than Sm-Nd. This is evident in some studies that compare Sm-Nd and Rb-Sr measured on the same sample aliquots where there can be greater scatter about a Rb-Sr isochron than for a Sm-Nd isochron (Edmunson et al., 2009). In addition to standard isochron chronology, coupled $^{146\text{-}147}Sm\text{-}^{142\text{-}143}Nd$ isotope systematics can be used to assess the mantle closure ages (i.e., the duration of lunar magma ocean crystallization) for the sources of lunar basalts (Boyet and Carlson, 2007; Brandon et al., 2009; McLeod et al., 2014). Finally, the nature and compositions of lunar mantle source compositions and potential mixtures can be assessed with the Sm-Nd system (Borg et al., 2009; Srivastava et al., 2022).

2.4 Lu-Hf

The Lu-Hf isotope system was first applied to lunar materials by Patchett and Tatsumoto (1981) and Unruh et al. (1984). Few subsequent papers presented Lu-Hf data (Beard et al., 1998) until the application of plasma-source mass spectrometry; now the Lu-Hf isotope system is routinely applied to lunar materials (Taylor et al., 2009; Sprung et al., 2013; Gaffney and Borg, 2014; Carlson et al., 2014; Melanie Barboni et al., 2017). The ^{176}Lu half-life used by the isotope geochemistry community changed from the value of 35.82 Ga (Patchett and Tatsumoto, 1980) to a value of about 37.12 Ga (Scherer et al., 2001; Söderlund et al., 2004), so care must be taken when comparing Lu-Hf isotope data and models in the literature. Hult et al. (2014) summarize many ^{176}Lu half-life measurements and propose a value of 37.22 ± 0.29 Ga.

The Lu-Hf isotope system is enhanced by the different geochemical behavior of Lu and Hf and resultant large range in $^{176}Lu/^{177}Hf$ ratios in many lunar materials. For example, most zircon has 1-3 wt% Hf and Lu in ppm concentrations resulting in $^{176}Lu/^{177}Hf$ ratios typically < 0.002. Combined with its robust retention of U-Th-Pb isotopes for precise chronology, zircon is also a powerful Lu-Hf isotope tracer requiring minimal age corrections (Taylor et al., 2009; Barboni et al., 2017). Phosphate minerals have the potential for $^{176}Lu/^{177}Hf$ ratios of over 100 (Amelin, 2005). Overall, in addition to zircon, many oxide minerals can have very low $^{176}Lu/^{177}Hf$ ratios of < 0.01, whereas phosphates and garnet have the potential for $^{176}Lu/^{177}Hf$ ratios greater than 1.0. Therefore, Lu-Hf mineral isochron chronology has the potential for relatively large spreads in Lu/Hf ratios even in lithologies with a simple mineralogy (e.g., Lapen et al., 2010).

Modern analytical methods for Lu-Hf chronology and/or isotope tracer studies include both in-situ laser ablation mass spectrometry and wet chemical approaches applied to bulk rock and/or mineral separates. Because Hf concentrations are in the ppb to ppm range for most rock-forming minerals, wet chemical approaches are required for analysis with minimum sample sizes typically of 0.05 to 0.10 g. Hafnium-rich minerals such as zircon and baddeleyite can be analyzed for Lu-

Hf isotopes by in-situ approaches (Ibanez-Mejia et al., 2014). All Lu-Hf isotope data of lunar materials should be assessed for neutron capture effects and corrected (Sprung et al., 2013; Gaffney and Borg, 2014; Barboni et al., 2017).

2.5 Ar-Ar

Turner (1970) presented some of the first applications of the $^{40}Ar/^{39}Ar$ method to Apollo 11 samples. Since then, $^{40}Ar/^{39}Ar$ data have been essential for unraveling the timing of primary and secondary lunar events such as protolith formation and impact metamorphism, respectively. Depending on the material and its temperature-time history, the $^{40}Ar/^{39}Ar$ method has the potential to provide precise dates of a wide-range of lunar materials (Turner et al., 1973; Turner and Cadogan, 1975; Dalrymple and Ryder, 1991, 1993, 1996; Jourdan, 2012; Fernandes et al., 2013). Impact events that produced melt can be precisely dated and help build impact flux estimates (Dalrymple and Ryder, 1993, 1996; Culler et al., 2000; Cohen et al., 2000; Kring and Cohen, 2002; Norman et al., 2006; Mercer et al., 2015, 2019; Zellner and Delano, 2015). The timing of lunar volcanism, often expressed as fine-grained and/or amorphous materials (e.g., lunar orange glass beads in 74220 soil), can be precisely dated (Huneke, 1978; Spangler et al., 1984; Zellner et al., 2009) whereas other isotope systems that rely on mineral-liquid fractionation processes would not typically yield precise age determinations of these bulk materials.

Potassium-40 has a branched decay to ^{40}Ca (89.32%) and ^{40}Ar (10.68%) with a total decay constant of about 5.53×10^{-10} yr^{-1} (Renne et al., 2011). Associated ^{40}K-^{40}Ca chronology of felsic lunar materials (Shih et al., 1993) is possible for specialized applications. Analytical details of the ^{40}Ar-^{39}Ar method are complex (McDougall et al., 1999; Cohen et al., 2000, 2005; Swindle et al., 2009; Weirich et al., 2010; Wittmann et al., 2011; Mercer and Hodges, 2016; Niihara et al., 2019; Schaen et al., 2020; Beard et al., 2022). Recent advancements in in-situ analytical approaches (Mercer et al., 2015) make it easier for analyses of critical petrographic contexts.

Argon-Ar thermochronology is especially useful for understanding the potentially complex temperature-time (T-t) history of lunar materials. For short T-t histories relative to the diffusivity of Ar in a particular material, Ar-Ar data may have remained a closed system since the last Ar-degassing event such as melting (Cohen et al., 2000). For T-t histories that are long and/or extreme enough to facilitate Ar loss, the timing of these Ar-loss events may be recorded in the measured Ar isotope data (Niihara et al., 2019; Schaen et al., 2020). Overall, Ar-Ar approaches, both in-situ and conventional, are a critical tool for unraveling primary and secondary processes operative on the Moon.

3 Lunar Lithologies

The Artemis exploration zone is a feldspathic highland terrain that was originally anorthositic crust, covered and/or mixed with more mafic lithologies excavated by the SPA and other basin-forming events producing a mixed - nominally noritic - composition (Pieters et al., 2001; Hawke, 2003; Spudis et al., 2008; Lin et al., 2020; Huang et al., 2020; Krasilnikov et al., 2023). Major minerals in the surface regolith are plagioclase, pyroxene, and olivine, in that order. Reflectance spectra suggest the region has an average anorthite abundance of ~80 to 90 wt% and ~5 to 10 wt % Fe) (Lemelin et al., 2022).

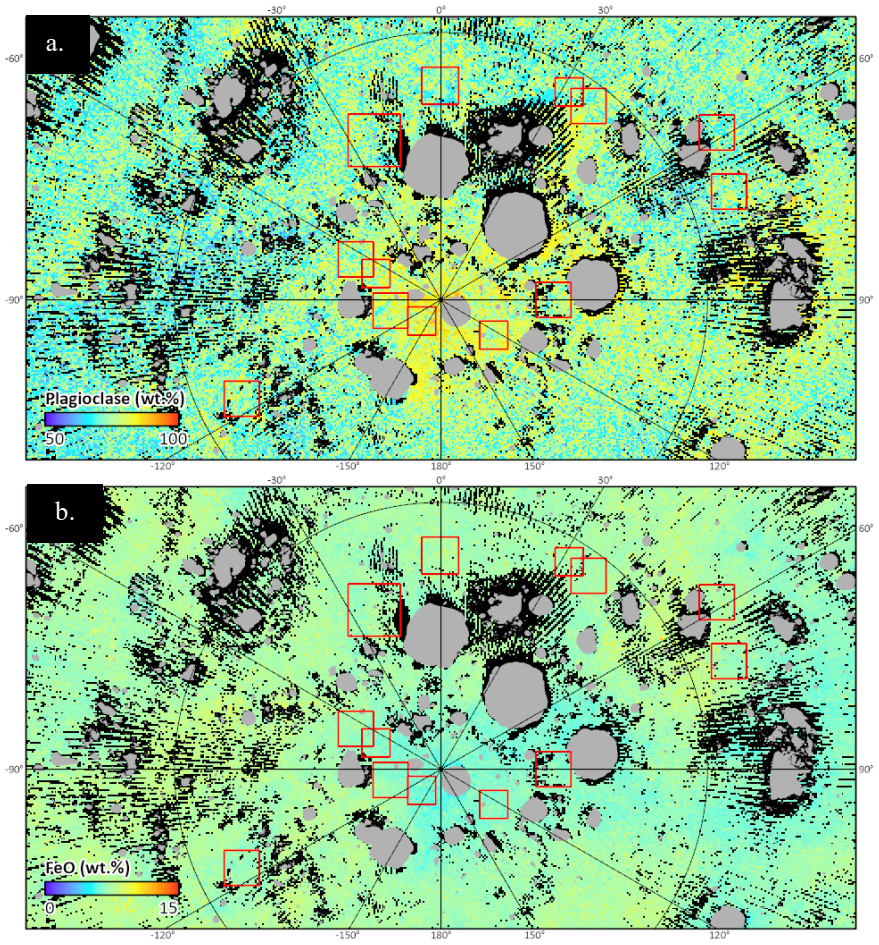

Figure 3. Colorized counts of Kaguya SP mineral data used to determine average lithological composition at each of the candidate landing regions (red squares). Gray areas represent permanently shadowed regions, which were masked during analyses. Black areas are areas with no mineral count data available. (**a**) Colorized counts of plagioclase from 50 to 100 wt. %. **(b)** Colorized counts of iron from 0 to 15 wt. %.

Table 2. Artemis zonal statistics of mineralogy at each landing site within an exploration zone of 10 radial kilometers. The values below contain minerals modeled from Spectral Profiler data with all PSRs masked from Lemelin et al. (2022). The four sites closest to the south pole (001, 004, 007, and 011) have similar mineralogy. The mineral error is on the order of ±8 wt. % and FeO about 2 wt. %. SD = standard deviation.

Site #	Lat.	Long.	FeO		Plagioclase		Low-Ca Pyroxene		High-Ca Pyroxene		Olivine	
			Mean	1 SD	Mean	1 SD	Mean	1 SD	Mean	1 SD	Mean	1 SD
001	-89.45	-137.31	6.2	0.4	81	5	10	6	0	2	9	6
004	-89.78	-155.73	6.1	0.4	83	4	8	5	0	1	9	6
007	-88.81	123.64	6.5	0.4	79	5	12	6	0	1	9	6
011	-88.67	-68.1	6.7	0.4	78	5	13	7	0	2	9	6
102	-85.55	37.57	7.2	0.3	74	5	19	7	0	1	7	5
105	-88.8	123.95	6.4	0.3	78	5	16	8	0	0	6	5

The basin-forming event that created SPA would have been an exceptionally violent impact (Potter et al., 2012) that excavated material from depth where mafic to ultramafic materials likely existed (Kring, 2005; Hurwitz and Kring, 2014), produced melt, fallback ejecta, and brecciated basin floor materials (Petro and Pieters, 2008; Moriarty et al., 2021). This, coupled with billions of years of subsequent impacts results in a complicated and varied lithological suite of outcrops and potential return sample targets. The lithologies discussed here are those which were defined by Stöffler et al. (1980) (Figure 4, Table 3). They may exist as homogenous hand samples (e.g., ~ 5 to 20 cm) or even at the outcrop scale, although there is a strong likelihood of polymict breccias housing a multitude of lithologies, much like NWA 5000 and various Apollo samples (Duncan et al., 1975; Grieve et al., 1975; Stöffler et al., 1985; Nagurney et al., 2016; Marks et al., 2019; Cao et al., 2021). Some lithologies, such as dunite (Shearer et al., 2015), are exceedingly rare within the Apollo collection and exist as chips and fragments within brecciated samples. Because it crystallizes at depth, dunite solely relies on impact excavation processes or incorporation into magmas as xenoliths to be exposed on the lunar surface. The spatial resolution of this study (>500 m) preclude identification of litho-fragments within an individual sample, driving the need for polymict breccia return samples.

We understand lunar rocks exist within a continuum of lithologies, however they are discussed below in accordance with the classification schema outlined in Figure 4. With the exception of impact melts or fine-grained basaltic clasts, we predict most lithologies in the Artemis exploration zone to be relatively coarse-grained (~1 to 3 mm grain size; Joy et al., 2008).

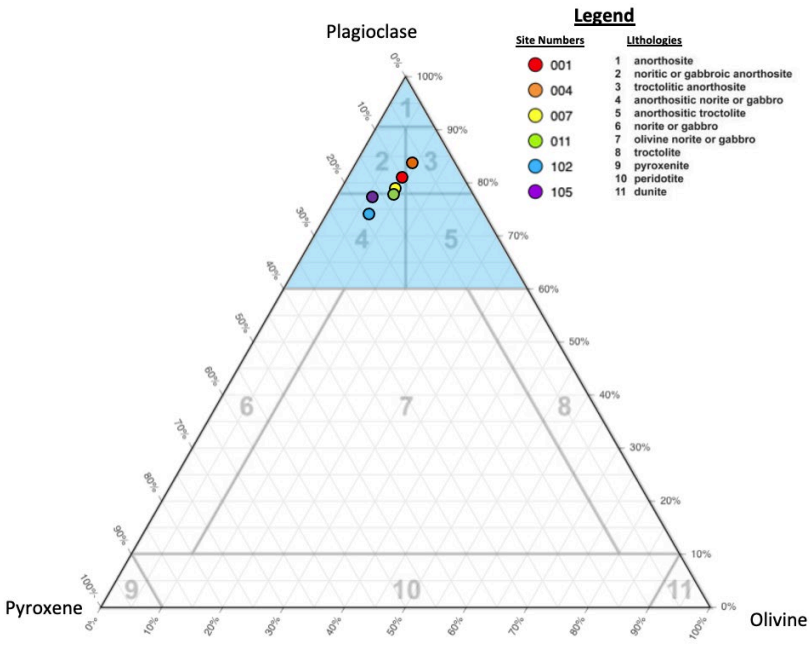

Figure 4. Average landing site lithological composition displayed relative to plagioclase, pyroxene, and olivine. Blue shaded region represents the zone of statistical uncertainty from our analysis. Modified after Stöffler et al. (1980).

Table 3. List of lunar lithologies that might be included in the regolith within each site. (List of lithologies from Hiesinger (2006)). Gray-filled boxes: within the standard deviation range of

453 average composition calculated from this study (PSRs not masked); X: presence of lithology
454 recognized; Y= existence of lithology likely, but below detection limit of current instrumentation;
455 Z: lithology possibly present as clasts. References: [1] Gawronska et al. (2020); [2] Lemelin et al.
456 (2022); [3] Yamamoto et al. (2012); [4] Uemoto et al. (2010); [5] Halim et al. (2021); [6] Ohtake
457 et al. (2009); [7] Borst et al. (2012); [8] Kraettli et al. (2022); [9] Gagnepain-Beyneix et al. (2006);
458 [10] Kring (2019); [11] Kring et al. (2022).
459

Lithology	Sites					
	001	004	007	011	102	105
Purest Anorthosite (PAN) [1-4]	Y	X	Y	Y	X	X
Anorthosite [1-3,5,6]	X	X	X	X	X	X
Noritic or Gabbroic Anorthosite [2]	X	X	X	X	X	X
Troctolitic Anorthosite [2]	X	X	X	X	X	X
Anorthositic Norite or Gabbro[2]	X	X	X	X	X	X
Anorthositic Troctolite[2]	X	X	X	X	X	X
Norite or Gabbro[2]	X	X	X	X	X	X
Olivine Norite or Gabbro[2]	X	X	X	X	X	X
Troctolite[7]	Y	Y	Y	Y	Y	Y
Pyroxenite[8,9]	Z	Z	Z	Z	Z	Z
Peridotite[7]	Z	Z	Z	Z	Z	Z
Dunite[7]	Z	Z	Z	Z	Z	Z
Basaltic material[7,10]	Z	Z	Z	Z	Z	Z

Impact Melt[10,11]	Z	Z	Z	Z	Z	Z
Impact Breccia[1,11]	Z	Z	Z	Z	Z	Z

460

461 ## 3.1 Anorthositic Lithologies

462 Anorthositic lithologies include anorthosite (and 'purest anorthosite') and noritic, gabbroic,
463 and troctolitic anorthosite. These lithologies are all characterized by having high proportions of
464 plagioclase with low, but variable proportions of pyroxene and olivine. Anorthitic plagioclase
465 tends to have relatively low concentrations of REE, K, Rb, and U, making direct chronometric
466 analyses difficult. The complex thermal and impact histories for many lunar anorthositic rocks
467 (see Shearer et al., 2006, and references therein) further compromises the accuracy and precision
468 of chronologic measurements. Despite these challenges, chronology of anorthositic rocks by U-
469 Pb of mafic phases, mineral and bulk-rock Sm-Nd, and Ar-Ar have been successfully
470 accomplished (e.g., Norman et al., 2003; Borg et al., 2011; Marks et al., 2019). Given the overall
471 low concentrations in alkali elements, Rb/Sr ratios are low, making Rb-Sr analyses of anorthositic
472 rocks useful as a petrogenetic tracer and for calculating model ages (e.g., Borg et al., 2022).

473 ### 3.1.1 Anorthosite

474 Anorthosites are coarse-grained igneous rocks that may record early lunar differentiation
475 processes. Anorthositic lithologies are common on the Moon because they may have formed from
476 early differentiation and crust-forming processes (Anderson et al., 1970; Wood et al., 1970; Wood,
477 1970; Ohtake et al., 2009). They are mineralogically defined as > 90 % by volume of plagioclase
478 (Figure 4), suggesting they are cumulates produced from an ancient melt (Lucey et al., 2006).
479 Mafic minerals in some lunar anorthosites have relatively low Mg/(Mg+Fe) ratios (Lucey et al.,
480 2006), and plagioclase within them is typically An_{96} which may reflect the Moon's depletion in
481 sodium and other volatile elements (Borg et al., 2022).

482 ### 3.1.2 Purest Anorthosite

483 A particularly pure anorthosite exists in the south polar region and is composed of >97 wt. %
484 anorthite with <2 wt. % pyroxene (Ohtake et al., 2009). Because it is almost pure anorthite, this
485 variant is known as 'purest anorthosite' (PAN) (Ohtake et al., 2009). Outcrops that correspond to
486 PAN spectra are recognized at the geographic south pole and extend into the massif bridging
487 Shackleton to de Gerlache crater (toward the west) and Slater crater (toward the east) (Gawronska
488 et al., 2020). The physical extent of the PAN unit is debated because no significant samples of
489 PAN were identified within the Apollo collection (Lemelin et al., 2015). Exposures of anorthosites
490 (90 to 100 wt. % plagioclase) are somewhat rare in the Artemis region, with a few concentrated
491 around Shackleton crater and on or near the ridge between Shackleton and Henson craters (~88.5
492 °S, 128 °W, near Site 004) (Lemelin et al., 2022). In this region, PAN could be intact and
493 crystalline, or potentially comprise portion of megabreccia with blocks 100 m in size (Gawronska
494 et al., 2020).
495 Small clasts of PAN might exist within lunar meteorites (Nagaoka et al., 2014), but PAN is not
496 known to exist within the Apollo collection. Some attribute the remote detection of PAN to an
497 erroneous calibration of spectral data (Warren and Korotev, 2022). The closest representative

sample is 97.6% An (mode) ferroan anorthosite 15415 ('Genesis Rock') (Steele and Smith, 1971; Wilshire et al., 1972; Turner, 1972), which formed after the Moon's crust solidified and, therefore, not representative of the LMO flotation crust remnants present in the south polar region (Ohtake et al., 2009). For direct testing of the earliest flotation crust products of lunar crust formation, PAN samples should be collected from the SPA, the oldest impact structure on the Moon.

PAN is mineralogically-pure in a scale detectable by remote sensing (Ohtake et al., 2009; Cheek et al., 2013; Donaldson Hanna et al., 2014; Lemelin et al., 2019). A potential opportunity to study the petrogeneses PAN materials could greatly improve the understanding of early lunar differentiation processes (Yamamoto et al., 2012; Gawronska et al., 2020; Kring et al., 2022). Return samples of PAN composition would help determine the spatial extent and composition of the primary feldspathic crust, improve our inventory of the variety of age, distribution, and origin of lunar rock types, aid in determining the composition of the lower crust and bulk Moon, and clarify the local and regional complexity of the current lunar crust (NRC Concepts 3a, 3b, 3c, 3d). Study of PAN return samples would aid understanding of how massifs were generated from the SPA basin-forming impact (Kring et al., 2020), and the successive geologic evolution of the region (NRC Concepts 1b, 1c). PAN samples may also provide an anchor to the early Earth-Moon impact flux curve by determining the age of the oldest lunar basin (SPA) (Kring, 2007; Mazrouei et al., 2019), establish a precise chronology of lunar geologic events (Marks et al., 2019), help determine the thickness of the lunar crust (Spudis and Davis, 1986), aid characterization of lunar crust variability on regional and global scales (NRC Concepts 1b, 1c, 2a). If anorthosite were to be collected in-situ from strata exposed on the massif cliff (pole-ward) side of Site 102, this would directly enable the investigation of the structure and composition of the lunar crust (Spudis and Davis, 1986; Kring et al., 2020) (NRC Concepts 2a, 2d). It would also reveal more about the multi-ring impact basin structure of SPA, quantify the effects of planetary characteristics (composition, density, impact velocities) on crater formation and morphology, and allow the extent of lateral and vertical mixing of local and ejecta material to be measured (NRC Concepts 6b, 6c, 6d).

3.1.3 Noritic, Gabbroic, or Troctolitic Anorthosite

Noritic/gabbroic anorthosites belong to the ferroan anorthosite (FAN) suite of lunar rocks and have been confirmed to exist within the SPA farside Highlands by analyses of the Chang'E-5 return sample CE5C0800YJYX132GP (Wang, 2022). Noritic/gabbroic anorthosite or troctolitic anorthosite (77.5 to 90 wt. % plagioclase, Figure 4) are the second most abundant lithologies in the south polar region (Lemelin et al., 2022).The parent melts of noritic/gabbroic anorthosites are believed to be produced during the lunar magma ocean (LMO) overturn by the decompression melting of upwelling Mg cumulates and coincident mixing with incompatible element enriched materials (e.g., potassium, rare earth elements, and phosphorous-rich; KREEP) (Hess and Parmentier, 1995; Elkins-Tanton et al., 2002, 2011). However, Apollo FANs are not representative of all lunar highland-type crust (Gross et al., 2014, 2020; Xu et al., 2020), so further study of noritic/gabbroic anorthosites returned by Artemis astronauts would provide information about the early evolution of the Moon as relevant to the LMO hypothesis.

Troctolitic anorthosite is an anorthosite with a minor olivine component (Figure 4) and the Mg# = 87 ± 5 (Lucey et al., 2006). Troctolitic anorthosite is a member of the magnesian suite (Mg-suite) of lunar lithologies and does not belong to the ferroan anorthosite (FAN) group of lunar lithologies (Lucey et al., 2006). It is representative of the average lithological composition of Site

004 (Lemelin et al., 2022). The collection of noritic or gabbroic anorthosite samples from the lunar surface would enable a more in-depth understanding of lunar crust formation and differentiation through the study of coexisting pyroxene and plagioclase, which is rare in other early LMO cumulates (Elardo et al., 2011). A better understanding of LMO crystallization trends from a more complete suite of materials that record this process will better inform thermal models of the Moon and the thermal state of the interior during early crustal formation periods (Shearer and Papike, 2005; Elardo et al., 2011) (NRC Concepts 2a, 2d) (NRC, 2007).

Noritic/gabbroic return samples would improve our understanding of the extent and composition of the primary feldspathic crust and other products of planetary differentiation, in turn quantifying the local and regional complexity of the current lunar crust (NRC Concepts 3a, 3c, 3d). This can be most accurately accomplished by collecting samples with known impact crater sources (i.e., in ejecta blankets with a clear crater source or in-situ from strata within crater walls). Certain samples may also enable clarification of the lateral rock type variability on regional and global scales.

Geochronological analyses of noritic/gabbroic anorthosites would improve the established global lunar time scale and timing of large impact basin formation (Wood et al., 1970; Hawke, 2003) (NRC Concepts 1b, 1c). Noritic/gabbroic samples will add to our efforts to inventory the diversity of lunar crustal rocks with respect to composition, age, distribution, and origin (NRC Concepts 3b, 3c). For example, should troctolitic anorthosite be collected from Shackleton ejecta, it would improve the understanding of early mafic cumulate products from the Lunar Magma Ocean (LMO), in particular the precipitation and equilibration of olivine within the lunar crust (Elkins-Tanton et al., 2011; Elardo et al., 2011) (NRC Concepts 3a, 3b, 3c, 3d). Direct sampling of troctolitic anorthosite could show how it was generated and preserved relative to the SPA basin-forming impact (Miljković et al., 2021) (NRC Concepts 1b, 1c, 2a, 3a, 3b, 3c, 3d), and the later geologic evolution of the region (NRC Concepts 1b, 1c) (NRC, 2007).

3.2 Mafic Lithologies

Lunar mafic lithologies include troctolite, norite, and gabbro, including anorthositic and olivine-bearing norite and gabbro. Many of these lithologies, especially coarse-grained varieties, contain a mineralogic diversity that allows for most chronologic systems in Table 1 to be applied. Methods involving Rb-Sr, Sm-Nd, and Lu-Hf isochron approaches have been applied (e.g., Borg and Carlson, 2023, and references therein). In many cases, important U-rich accessory phases such as zircon, baddeleyite, and phosphate group minerals are present, allowing for in-situ chronology by laser ablation and ion probe (e.g., Shaulis et al, 2017; Merle et al., 2020).

3.2.1 Anorthositic Norite, Gabbro, or Troctolite

The regolith of the south polar region is dominated by anorthositic noritic/gabbroic and anorthositic troctolitic mineral spectra (Lemelin et al., 2022). Of that regolith, anorthositic norite/gabbro and anorthositic troctolite (60 to 77.5 wt. % plagioclase with varying proportions of clino- to orthopyroxene, Figure 4) were identified at sites 011, 102, and 105 (Lemelin et al., 2022). Anorthositic troctolite is an igneous rock with more plagioclase component than traditional troctolite (Figure 4) It is still unknown if anorthositic troctolites from the AEZ will be coarse- or

fine-grained. Anorthositic troctolites from SPA may signify lithologies formed very early on in lunar history (Lucey et al., 2006).

If anorthositic norite/gabbro or anorthositic troctolite were to be collected from the Artemis region, those samples may illuminate how differentiation occurred after the overturn of the LMO including a better characterization of the thermal state of the interior (Elkins-Tanton et al., 2011; Elardo et al., 2011) (NRC Concepts 2a, 2b, 2d). These differentiation products are valuable tools to understand more details of the extent and composition of varied lithologies, and to quantify our inventory of the nuanced complexities therein (i.e., variety, age, distribution, origin) (NRC Concepts 3a, 3b, 3d) (NRC, 2007). Anorthositic norite/gabbros may also aid in the understanding of the bombardment history of the inner solar system recorded within the uniquely preserved lunar crust in samples with impact-reset ages (Kring, 2019). This would allow for the anchoring of the impact flux curve, determining the cadence of the creation of lunar basins (Kring, 2007), and establishing a precise absolute chronology of the geologic evolution of the lunar south pole region (NRC Concepts 1a, 1b, 1c).

3.2.2 Gabbro and Norite

Gabbro is a general term for a coarse-grained (typically plutonic) mafic igneous rock composed of plagioclase, Ca-rich clinopyroxene (augite), and <5 wt% of each of olivine and orthopyroxene (Figure 4). Norite is an orthopyroxene-bearing gabbro, with < 5 wt. % clinopyroxene or olivine (Figure 4). Lunar norites are distinguished from lithologies termed ‘gabbronorites’ by the absence of a discrete high-Ca pyroxene phase and presence of a wider variety of trace phases (Papike et al., 2006). Because Shackleton crater is on the edge of the SPA basin, target material of Shackleton may be ancient noritic crust which may be exposed within crater walls (Gawronska et al., 2020). Gabbro/norite lithologies in SPA are believed to originate from upper mantle ejecta and contain a high abundance of Th- and K-bearing materials (Moriarty et al., 2021).

Gabbros and other mafic lunar lithologies can be used to define magmatic periods and chemical characteristics of mantle components contributing to the sources of the magmas (Papike et al., 2006). Gabbroic/noritic cumulates may not have participated in the gravitational overturn during the time of SPA formation (Moriarty et al., 2021), so return samples of this type would reveal critical information about magmatic differentiation events in early lunar history (NRC Concepts 2a, 2b, 2d, 3a, 3b, 3d).

If gabbro or norite were to be collected from the Artemis region, it would aid in understanding the diversity of lunar crustal rocks through the comparison with Apollo samples of similar composition (NRC Concepts 3a, 3b, 3c, 3d, 6c, 6d). The large-scale lateral and vertical distribution of gabbro/norite lithologies could be better determined through in-situ observations of strata in crater walls and determination of source magmas via geochemical study (Shaulis et al., 2017). Defining isochron ages from analyses of these pyroxene-rich lithologies would aid in the understanding of the bombardment history of the inner solar system recorded within the lunar crust (Shih et al., 1993; Norman et al., 2003; Carlson et al., 2014; Zhang et al., 2021) (NRC Concepts 1a, 1b, 1c, 3a, 3b, 3c, 3d). Gabbro/norite analyses could also show how magmatic events, including differentiation, transpired after the LMO overturn (NRC Concepts 2a, 2b, 2d, 3a, 3b, 3d) (NRC, 2007).

3.2.3 Olivine Norite or Gabbro

Olivine norite or gabbro are composed of 10 to 50 wt. % plagioclase with varying proportions of olivine and pyroxene (Figure 4). This lithology is included in the Mg-suite of lunar rocks, which is representative of the crustal growth and basaltic magmatism period in lunar history (Shearer and Papike, 2005). The Chinese lunar farside mission Chang'E-4 identified a rock of olivine norite composition that is believed to have crystallized from the SPA impact pool using a visible and near-infrared spectrometer aboard the Yutu-2 rover (Lin et al., 2020). Although olivine norite/gabbro is not a dominant lithology within a 10-km radial exploration zone from any of the six potential crewed Artemis landing sites, fragments of it could be entrained in breccias. The Yutu-2 rover discovery of an olivine norite greatly increases the likelihood of finding others like it within SPA on the lunar nearside. Compositions consistent with olivine norite have been recognized but those compositions can also represent clast contamination in breccia (Lemelin et al., 2019). Olivine norite has also been recognized to exist as the most abundant host lithology of olivine on the edges of the innermost ring material of several basins (e.g., Moscoviense, Humorum, Imbrium, and Serentitatis), although may represent 'contamination' from basaltic materials (Yamamoto et al., 2010; Lemelin et al., 2019).

If olivine norite/gabbro were to be collected from the Artemis region, it would shed light on impact kinematics and 'contamination' effects within impact structures (Lemelin et al., 2019), reveal a more detailed record of the bombardment history of the inner solar system recorded within the lunar crust (NRC Concepts 1a, 1b, 1c, 3a, 3b, 3c, 3d), and add valuable information to the diversity of lunar crustal rocks in an impact terrane (NRC Concepts 3a, 3b, 3c, 3d, 6c, 6d) (NRC, 2007). The higher proportions of olivine within an olivine norite or gabbro would allow for more opportunities to investigate early differentiation processes within the lunar crust.

3.2.4 Troctolite

Troctolite is composed of plagioclase and olivine, with < 5 wt. % of pyroxene (Stöffler et al., 1980; Prissel and Prissel, 2021). Troctolites are included in the "Mg-suite" of nonmare lunar rocks and analyzed specimens contain a whole rock composition of Mg # = 87 ± 5. Troctolites are the most abundant Mg-suite sample type in the Apollo collection (Shearer et al., 2015), but the spatial distribution on a global scale is not well understood.

Troctolites may represent the start of mantle materials in a subsurface depth profile (Hess, 1994). An olivine-bearing lithology, possibly troctolite, is abundant in the peak-ring of the Shrodinger basin near the Artemis exploration zone. The original spectroscopy was published by Kramer et al. (2013). An LRO picture showing many kilometers of rock exposure in the peak ring was published by Kring et al. (2017). Hydrocode calculations indicate the olivine-bearing lithology was uplifted from depths of 20 to 30 km (Kring et al., 2016). Previous study of phosphorous diffusion patterns within olivine grains within lunar troctolite 76535 revealed a two-stage cooling model (initial rapid cooling at high temperatures, then slow cooling at lower temperatures) (Nelson et al., 2021). Therefore, continued study of lunar troctolites in impact ejecta or fragments of troctolites harvested from polymict breccias would lead to greater understanding of the thermal history of the Moon. However, if troctolite were to be collected from in-situ outcrops within crater walls, it would provide the most detailed context of the specific landing site's history through the observation of geologic relationships and large-scale textures. Because the global distribution of

673 Mg-suite lithologies is still unknown, the sampling of troctolite (or another in-situ mafic lithology)
674 could bring more understanding to their spatial extent and source regions (Shearer et al., 2015).
675
676 If troctolite were to be collected from impact ejecta or otherwise, it would allow for the creation
677 of a more detailed absolute chronology of serial magmatism, crust/mantle formation and evolution,
678 and impact and degassing events (McCallum et al., 2006; Elardo et al., 2012; Shearer et al., 2015;
679 McCubbin and Barnes, 2020) (NRC Concepts 1a, 1b, 1c, 1e). Troctolite samples would improve
680 the understanding of the structure and composition of the lunar interior, including a potentially
681 stratified upper mantle (Moriarty et al., 2021) (NRC Concepts 2a, 2b, 2d), and elucidate the nature
682 of the lower crust-mantle boundary (NRC Concepts 3a, 3b, 3c, 3d) (NRC, 2007).

683 ### 3.3 Ultramafic Lithologies

684 Lunar ultramafic lithologies include pyroxenite, peridotite, and dunite. These lithologies are
685 typically incompatible trace-element (ITE) depleted, thus rock and mineral compositions can be
686 low in REE, U, K, and Rb. Depending on the mineralogy and ITE compositions, Rb-Sr, Sm-Nd,
687 and Lu-Hf have be applied to certain martian and terrestrial ultramafic specimens (e.g., Lapen et
688 al. 2005; 2010). Currently, lunar ultramafic rock specimens are extremely rare but are extremely
689 important for unraveling the timing of early lunar differentiation.

690 #### 3.3.1 Pyroxenites

691 Pyroxenite is a cumulate, igneous rock comprised of >90 wt. % pyroxene (Figure 4). It is
692 believed to be representative of lunar upper mantle layers crystallized directly from the LMO, and
693 thus difficult to observe in-situ due to a mostly subsurface existence (Gagnepain-Beyneix et al.,
694 2006; Kraettli et al., 2022). Despite the presence of deep craters within SPA, pyroxenite is not
695 currently known to be present at outcrop-scale within the Artemis region, which may be a relic of
696 the generally coarse spatial resolution of spectral data. Pyroxenite may, however, have been
697 excavated from depth and exist at the surface as lithic fragments within brecciated hand samples
698 within the Artemis region.
699
700 If pyroxenite were to be collected from impact ejecta, it would improve the understanding of
701 the structure and composition of the lunar interior (NRC Concepts 2a, 2b, 2d), elucidate the nature
702 of the lower crust-mantle boundary (NRC Concepts 3a, 3b, 3c, 3d), and reveal a more detailed
703 absolute chronology of impact events that led to the formation of SPA (NRC Concepts 1a, 1b, 1c,
704 1e) (NRC, 2007).

705 #### 3.3.2 Peridotite

706 Peridotite is an olivine-rich (Figure 4) cumulate igneous rock that is not yet known to exist
707 within the SPA region, however olivine-rich exposures have been identified throughout SPA
708 (Pieters et al., 2001; Yamamoto et al., 2010, 2012). Although it is not yet known to exist in sizable
709 deposits identifiable by current detection limitations, the possibility of a peridotite fragment
710 existing in a brecciated sample remains.
711
712 If peridotite were to be collected from impact ejecta, it would improve the understanding of
713 the composition of the lunar mantle and therefore, increase knowledge of structure and
714 differentiation in the lunar interior (NRC Concepts 2a, 2b, 2d), allow interpretation of the nature

of the lower crust-mantle boundary (NRC Concepts 3a, 3b, 3c, 3d), and reveal a more detailed absolute chronology of impact events, specifically the formation kinematics of the SPA basin (NRC Concepts 1a, 1b, 1c, 1e) (NRC, 2007).

3.3.3 Dunite

Dunite is composed of 90 to 100 vol. % olivine (Figure 4). Olivine exposures have been detected within walls, ejecta, and peaks of craters within the SPA basin (Yamamoto et al., 2010). It is unclear whether the exposures were excavated upper mantle (dunite) material or Mg-rich plutonic material (troctolite) in the Moon's lower crust (Yamamoto et al., 2010). Deep-seated olivine-rich layers would be hidden by a differentiated impact melt sheet (Grieve et al., 1991; Nakamura et al., 2009; Hurwitz and Kring, 2014), but later impacts could have excavated and exposed the olivine. This olivine-rich lithology is best observed at young, fresh craters in the concentric regions around large basins (Yamamoto et al., 2010). It is possible the SPA impact may have excavated into the mantle (Lucey et al., 1998), although it would have reprocessed the material in some manner (e.g., giant, differentiated impact melt sheet (Hurwitz and Kring, 2014).

Very little ultramafic material exists within the Apollo collection. The only sample large enough to make the parent rock known (dunite fragments 72415-72418) has been extensively crushed and shows a complex history of shock, deformation, and recrystallization (Albee et al., 1974; Dymek et al., 1975; Lally et al., 1976; Papike et al., 2006). Dunite is representative of lunar mantle materials. The collection and return of in-situ lunar dunite to Earth would be a significant finding, as none of this yet exists in the lunar collections and is only hypothesized to exist in select areas within SPA. If dunite were to be collected from outcrop, it would improve the understanding of the structure and composition of the lunar interior (NRC Concepts 2a, 2b, 2c, 2d), however this scenario is unlikely because dunite exists at depth and would not easily be exhumed. If dunite is present within the Artemis exploration zone, it most likely exists as fragments and chips within ejecta blankets produced via impact cratering processes significant enough to reach the lunar mantle depths (Vaughan and Head, 2014; Moriarty and Pieters, 2018).

Any lunar dunite would be a unique and rare addition to the lunar collection and could increase our knowledge of the diversity of lunar crustal rocks (NRC Concepts 3a, 3b, 3c, 3d). Because it would have been excavated from depth via large impactor, it could a) act as a 'probe' to examine mantle lithologies and petrologic evolution of the lunar interior, and b) highlight information about the bombardment history of the inner solar system (NRC Concepts 1a, 1b, 1c, 1e) (NRC, 2007).

3.4 Basaltic Materials

Basaltic materials are fine-grained mafic rocks that display a wide range in compositions similar to the suite of mafic plutonic rocks described earlier. Understanding the ages of these materials constrains the volcanic history of the Moon. Some basaltic materials have U-rich accessory phases that can be dated in-situ or can be dated by the Pb isotope systematics of other igneous phases (e.g., Curran et al., 2019; Li et al., 2021). In many cases, and where the rock has a relatively simple thermal history, Ar-Ar chronology has the potential for precise determinations of eruption ages.

Photogeologic studies and return samples confirmed the lunar mare areas are formed by large volumes of flood basaltic lava, like the Columbia River Basalts on Earth (Wilson and Head, 1981).

Although no traditional mare materials are confirmed to exist at the surface in SPA, it likely resides in considerable quantities at depth in this region and is known as cryptomare. Cryptomare is basaltic in composition and represents some of the earliest volcanism on the Moon that has been buried by the later emplacement of crater ejecta material and basin-forming events (Head and Wilson, 1992). Cryptomare within SPA is estimated to cover a minimum area of 2.5 x 10^5 km^2, be at least 400 m thick, volumetrically encompass >1.0 x 10^5 km^3, and be 3.63 to 4.1 Ga (Shearer et al., 2006). Cryptomare is observed within SPA through examination of dark-haloed craters (Schultz and Spudis, 1983) which enable the darker albedo cryptomare to be studied against the lighter albedo regolith materials. In-situ cryptomare exposures may not be present or accessible at any of the six potential landing regions but may still be present within the Artemis exploration zone as hashed fragments within crater ejecta. Impact melt ponds also exist on the margins of craters and are composed of basaltic 'mare' material, though they are not the classical mare deposits we were familiarized with from the Apollo landing sites.

If basaltic materials were to be collected in-situ from 'cryptomaria' strata within crater walls, application of geochronology methods would primarily reveal vital information about early lunar volcanism including the lunar volcanic flux, mantle sources, and compositional variability of basalts (NRC Concepts 5a, 5b, 5d). Impact melt ponds may also be sampled in-situ from the outer margins of craters within the Artemis region but would be more telling of the bombardment history of a region than a distinct new type of volcanism generated from depth (NRC Concepts 1a, 1b, 1c, 1e). Collecting 'mare' type materials from impact ejecta would also prove useful toward establishing absolute chronology (NRC Concept 1c), broaden our understanding of the diversity of lunar crustal rocks (NRC Concept 3a, 3b, 3d), and reveal limited information on lunar volcanism (NRC Concept 5a, 5b, 5d) (NRC, 2007).

3.5 Impact Melts

Impact melt is created by intense shock pressures and temperatures that result in instantaneous melting and rapid quenching of a rock during impact. The original rock bulk chemistry is preserved, but the mineralogy and petrography is destroyed to varying degrees (Kettrup et al., 2003). Chronology of these materials typically rely on systems that are susceptible to thermal disturbances and systems (e.g., Ar-Ar) that can be applied to melts (Turner, 1972; Turner et al., 1973; Dalrymple and Ryder, 1993, 1996; Zellner and Delano, 2015; Norman et al., 2019) . Distinctions between impact melt, impact glasses, and volcanic glasses are important. Impact glasses are similar to volcanic glasses but are instead associated with shock and metamorphosed lithic fragments. Impact melt fragments are found in breccia deposits within and outside impact craters ('suevite'), and as spherules in distal ejecta ('tektites') (Dressler and Reimold, 2001). Impact melt rocks differ from impact glasses in that they occur as massive bodies of rock crystallized from melt bodies, commonly in the form of sheet-like masses, in the interior of some impact craters.

Most impact-melt rocks contain lithic and mineral clasts from the target (Dressler and Reimold, 2001 and references therein; Stahle, 1972), which show clear shock and thermal effects (Bischoff and Stöffler, 1984). Complete homogenization of a target rock is only achieved in impacts by vaporization and whole-rock melting. The shock pressures required to produce whole-rock melting of gabbro is >75-80 GPa, dunite is >60-70 GPa, and most relevant to SPA, anorthosite is >45-50 GPa (Müller and Hornemann, 1969; Stöffler and Hornemann, 1972; Stöffler, 1974;

Reimold and Stöffler, 1978; Schaal et al., 1979; Ostertag, 1983; Bischoff and Stöffler, 1992). Material identified as impact melt composes 30-50% of all hand-specimen-sized rocks returned from highland landing sites and ~50% of all lunar soil materials, including non-mare collections (Ryder, 1981). Impact-melt rocks from the parent crater are the most reliable for dating the time of impact (Staudacher et al., 1982; Stephan and Jessberger, 1992; Deutsch and Scharer, 1994) and should be the first choice for any dating effort.

The SPA impact likely formed from a 170 km diameter impactor with an energy of $\sim 4 \times 10^{26}$ J, replacing the basin center with a melt pool of mantle-dominated composition (Potter et al., 2012). This large melt pond would have cooled slow enough to differentiate within itself, creating a differentiated melt sheet within SPA, and therefore the Artemis region (Hurwitz and Kring, 2014). Sampling of different locations (e.g., quenched margins vs. strongly differentiated center) of the SPA impact melt sheet would reveal a more detail about the impact, its age, and thermal history of the Moon.

Sampling of varied locations of a differentiated melt sheet within SPA would uniquely enable fundamental information about impact processes including melt sheet differentiation (Hurwitz and Kring, 2014) (NRC Concepts 6a, 6b, 6c, and 6d), make a distinct and diverse addition to our current sample collection of lunar crustal rocks (NRC Concepts 3a, 3b, 3d), aid in untangling the bombardment history of the inner solar system (Kettrup et al., 2003; Lin et al., 2020) (NRC Concepts 1a, 1b, 1c), and better constrain the thickness and variability of the lunar crust within SPA (Wieczorek and Zuber, 2001; Besserer et al., 2014) (NRC Concepts 2a, 2b). Impact melt fragments collected from ejecta would reveal impact event timing in the Artemis region, although in some cases it may be difficult to identify the source crater of the melt.

3.6 Impact Breccias

Impact breccias can contain a wide assortment of lithologies, a range in textures, materials with wide ranges in thermal histories, and contain clasts from various locations/levels in the Moon. Because of this variability, thus the chronologic opportunities can be rock/clast specific. Due to the classification of SPA as an impact terrain, a significant fraction of the surface lithologies available to Artemis astronauts and robotic assets will be breccias. Impact breccias are composed of older rocks that have been broken or melted by meteoroid impact (Stöffler et al., 1979). The components of breccias may be mineral and lithic fragments, crystallized impact melt, or glassy impact melt. Despite their randomized nature of rock and mineral components generated by impacts, they are lithified by the heat and shock associated with the impact. Most of the rock fragments in breccias of the distal part of the continuous ejecta deposits are from the local bedrock (Deutsch and Stöffler, 1987; Stöffler and Ryder, 2001).

A melt rock with clasts of unmelted (potentially shock-metamorphosed) targeted material is an ‘impact melt breccia.’ These melt bodies may intrude into fractures on the crater floor as veins and dikes that have been resampled by later impact events (Dressler and Reimold, 2001). Conversely, breccias composed of exclusively clastic components are ‘fragmental’ or ‘lithic’, and allow for the possibility to identify the nature of their dominant source rock types (Dressler and Reimold, 2001). The lithology, texture, and clast-types within breccias can be so widely varied that they, as a group, host the potential to address a majority of the NRC (2007) concepts. For example, a single polymict impact breccia could contain fragments from units with the ability

reveal the age of the SPA basin (NRC Concepts 1b, 1c), record a history of the ancient thermal state of the lunar interior (NRC Concept 2d), contain a wide diversity of lithologies (e.g., polymict breccias) (NRC Concepts 3a, 3b, 3c, 3d), host a cryptomare clast (NRC Concepts 5a, 5b, 5d), host a clast from a specific impact-associated unit such as a differentiated melt sheet (NRC Concepts 6a, 6b, 6c), and exist as a mixture of units from depth and local ejecta and regolith materials (NRC Concepts 6d, 7a, 7c, 7d). Breccias are common to find in impact terrains but vary greatly in their contents. Each brecciated sample will require a highly individualized approach to the analyses and assessment of applicable NRC Concepts (2007).

3.7 Regolith Breccias and Soils

The lunar regolith was created by large impacts which reduced the grain size of the underlying bedrock (Horz et al., 1991; McKay et al., 1991). This regolith layer records the Moon's impact history and the nature and timing of material delivered to the Moon's surface (e.g., Lucey et al., 2006). Due to the high velocity of impact (e.g., Le Feuvre and Wieczorek, 2011) and resultant melting and/or vaporization, a projectile imparts its geochemical signature into impact melt deposits it creates (Morgan et al., 1972a, b; Ganapathy et al., 1974; Higuchi and Morgan, 1975; Gros et al., 1976; James, 1996, 2002; Norman et al., 2002; Puchtel et al., 2008). However, some impactors completely or partially survive the lunar impact process intact, as evidenced by unmelted fragments of meteorites that have been found in lunar rocks and soils (e.g., McSween Jr, 1976; Jolliff et al., 1993; Zolensky et al., 1996; Rubin, 1997; Zolensky, 1997; Day et al., 2006). When paired with a time of impact, these partially unmelted samples help to provide better geochemical and chronological constraints for models of Solar system dynamics and causes of impact spikes to the Earth-Moon system (Turner et al., 1973; Tera et al., 1974; Dalrymple and Ryder, 1993, 1996; Cohen et al., 2000; Kring and Cohen, 2002; Kring et al., 2005; Norman et al., 2006; Ćuk et al., 2010). Geochemical and chronological evidence from lunar samples informs our understanding of the Earth-Moon system, and the wider inner Solar system. Ages of lunar regolith breccias and soils can be estimated from the trapped $^{40}Ar/^{36}Ar$ ratio of a sample. The abundances of trapped ^{40}Ar within a regolith sample is normalized to ^{36}Ar as an indicator of the point in time of the last exposure to solar wind (i.e., the space environment), before closure of the system through burial by an ejecta blanket or a basalt flow. Variations of trapped Ar with time has been used to estimate the ages of lunar regolith samples (Eugster et al., 1980, 1983, 2001; McKay et al., 1986; Eugster and Polnau, 1997). A model age representing breccia closure represents the last time grain-size components of the breccia were exposed to solar wind and may be used to calculate the formation time of the breccia (Joy et al., 2011, after Eugster et al., 2001). The technique was used to determine the ages of 191 lunar regolith samples from Apollo, Luna, and meteorite collections (Fagan et al., 2014).

In addition to what was stated in the impact breccia section, regolith breccias and lunar soils have the potential to address physical properties of the extremely cold (and possible volatile-rich) polar regolith (NRC Concept 4d), measure the extent of lateral and vertical mixing of local and ejecta material (NRC Concept 6d), and utilize the Moon as a natural laboratory for regolith processes and weathering on anhydrous airless bodies (NRC Concepts 7a, 7b, 7c, 7d).

4 Chronologic Applications: Limitations and Opportunities

In the previous sections, the Artemis exploration zone lithologies are described and the science potential for these returned materials is discussed. Applications of chronologic approaches to these lithologies and some specific and unresolved major questions are informed by previous chronologic studies (Nyquist and Shih, 1992; Nyquist et al., 2001; Carlson et al., 2014; Borg et al., 2015; Barboni et al., 2017; Papike et al., 2018; Borg and Carlson, 2023). A primary question is: what is the age of the Moon? This seemingly simple question has been exceedingly difficult to answer.

4.1 Age of the Moon and timing of the LMO

In the context of a Moon-forming impact model of Lock et al. (2018), the violence of this event served to destroy most, if not all evidence of the impactor and proto-Earth. The Moon would have formed from a terrestrial synestia and undergone a magma ocean phase (Elkins-Tanton et al., 2011; Elardo et al., 2011). During the lunar magma ocean (LMO) crystallization phase, metal-silicate differentiation would take place. The timing of lunar core formation is robustly constrained to have occurred after 4.51 to 4.50 Ga based on the short-lived ^{182}Hf-^{182}W isotope system (Touboul et al., 2007; Kruijer and Kleine, 2017). Thus, the Moon formed *after* 4.51 – 4.50 Ga. Constraints on the first silicate minerals to form in the crust and mantle during the magma ocean crystallization phase is where significant debate exists. Prominent, accessible lithologies that should reflect LMO fractionation products are anorthositic flotation cumulate rocks that form after about 75% of the LMO crystallized (Rapp and Draper, 2018). As discussed in Borg and Carlson (2023), numerous attempts to date lunar anorthosites have yielded many different results. They discuss many issues that could result in 'excess' scatter about an isochron (meaning that the scatter is greater than predicted from analytical uncertainties alone) and initial isotopic compositions that suggest open-system behavior or variable effects of secondary processes. Thus, Borg and Carlson (2023) suggest that the most reliable ages are those that are supported by independent confirmation with another isotopic system and from these criteria conclude that anorthosites related to LMO crystallization are likely no older than about 4.36 Ga. There are, however, other studies that show relatively robust isochrons indicative of older ages but lack independent confirmation. These include a Sm-Nd mineral and whole rock isochron age of 4.463 ±0.040 Ga in Descartes breccia 67215 (Norman et al., 2003), an Sm-Nd isochron age of 4.436 ±0.034 for an anorthositic clast in Y-86032 (Nyquist et al., 2006). The oldest reliable age determined directly from a ferroan anorthosite constrains how late the Moon-forming event was. The potential for additional anorthositic materials from the Artemis explorations areas, especially the potential PAN lithologies, may provide materials that could help better constrain the timing of LMO crystallization and the age of lunar formation, overall. Other constraints on the age of the Moon come from Lu-Hf model ages of lunar zircon (Barboni et al., 2017). These data provide strong evidence that the Moon-forming event occurred at about 4.50-4.51 Ga and highlight an 'old versus young' Moon formation debate. Collection of any materials containing zircon (e.g., gabbroic clasts) in the exploration zone can further test the Lu-Hf constraints on lunar formation.

In addition to the sample return of materials that may help directly date the Moon-forming event through an expanded sample suite, new analytical opportunities are evolving. These include advances in in-situ Rb-Sr isotopic analyses (Dauphas et al., 2022; Zhang, 2022). Because anorthositic lithologies are susceptible to disturbance and have experienced protracted thermal

histories that may have resulted in isotopic disequilibrium (Borg and Carlson, 2023), in-situ approaches have the potential for identifying sample areas (e.g., in a thick or thin section) that are disturbed and those that are more pristine. This information will be invaluable for identifying lunar materials that best preserve their primary or protolith components and target those areas for dating. Robust ages, as defined by Borg and Carlson (2023), determined directly from LMO products will have major implications for lunar age models and the timing and duration of the LMO.

Another way to date the LMO is to assess the formation timing of lunar mantle sources. A robust method to determine when the lunar mantle ceased evolving through LMO crystallization processes is to investigate the ^{146}Sm-^{142}Nd and ^{147}Sm-^{143}Nd isotopic compositions of lunar materials (Nyquist et al., 1995; Boyet and Carlson, 2007; Borg et al., 2019). These studies show that the lunar mantle closed to fractionation at about 4.33 Ga, but these data do not constrain when LMO crystallization began. Thus, additional constraints on the timing of LMO crystallization can be made if additional LMO products were collected and returned, such as those that may have been excavated from depth during the SPA impact (Potter et al., 2012; Hurwitz and Kring, 2014; Garrick-Bethell et al., 2020; Lin et al., 2020; Moriarty et al., 2021).

4.2 Timing of Lunar Magmatism

Lunar magmatism has been ongoing until at least 2.030 ±0.003 Ga (Li et al., 2021). Models that explain the evolution of lunar magmatism through time are underpinned by robust chronology. While anorthositic rocks are often associated with LMO processes, lunar magmatism is often associated with materials that are more basaltic in composition. Because these materials (which include mare basalt, cryptomare, and most Mg-suite rocks) have more diverse mineralogies than anorthositic rocks, the chronologic opportunities are far greater and essentially encapsulate all of the systems and approaches listed in Table 1. Of critical note, trace U-rich phases such as zircon and baddeleyite have the potential for precise U-Pb ages, even in thermally and chemically disturbed specimens. In thermally undisturbed specimens and/or fine-grained or amorphous specimens, precise Ar-Ar chronology can yield precise magmatic age determinations (e.g., Jourdan, 2012 and references therein). Precise mineral isochrons have been successfully applied to numerous basaltic lunar compositions coarse enough for mineral separations (Nyquist and Shih, 1992; Rankenburg et al., 2007; Carlson et al., 2014). Given that most of the compositional mapping noted in section 2 indicates anorthositic compositions, mafic clasts could be present that are below the spatial resolution of spectral mapping. Thus, mafic lithologies have relatively high probabilities of success for chronology and these data can better inform models for the magmatic evolution of the Moon and help develop thermal models that explain at least ~2.5 billion years of lunar magmatic activity.

4.3 Impact Processes and the Age of SPA

The Artemis exploration zones are located within the SPA basin and within heavily impacted terrain. It is expected that most materials collected from these regions will have been affected to some degree by impact processes. Figure 2 summarizes some of the predicted geology and unit ages that might be encountered in the exploration zones. Critical to assessing the source(s) of ejecta and their impact ages, dating impact metamorphism and/or impact melting is required. Standard approaches involve Ar-Ar analyses of impact glass or material that experienced significant Ar-loss during impact metamorphism. Materials that crystallized from an impact melt

can have U-rich phases that can be dated by in-situ U-Pb analyses or can be dated by mineral isochron approaches. In most cases, specimens that developed through impact processes can be dated in a variety of ways depending on the severity of impact metamorphism/melting; often, both the age of the protolith and the age of thermal metamorphism can be established (Burgess et al., 2007; Fernandes et al., 2013; Shaulis et al., 2017; Černok et al., 2021). The opportunity that impact materials would be collected from mapped terrains, connections between ejecta and impact basin can be strengthened. For impact chronology, the limit on science return is not the analytical techniques, it's the nature and types of samples collected from the surface and how they relate to the surface geology.

5 Sampling Strategy

The lithologies detected in the Artemis region by numerous previous studies (Yamamoto et al., 2012; Lemelin et al., 2017, 2022) were identified at relatively coarse spatial resolutions (1 km/pixel; 500 m/pixel). It should be noted that two upcoming instruments with improved spatial resolution (Imaging Infrared Spectrometer aboard Chandrayaan-2; High-Resolution Volatiles and Minerals Moon Mapper aboard Lunar Trailblazer) will launch prior to crewed Artemis activities. Both instruments will produce data at a spatial resolution of 70 to 80 m/pixel, which will dramatically increase the mineralogical detail available to identify less abundant lithologies (i.e., PAN, olivine-rich units, mafic lithologies, etc.).

The Apollo astronauts were instructed to collect the greatest diversity of samples with the coarsest grain sizes to allow for easier mineral separation in laboratory analyses on Earth (Phinney, 2015). This practice does not need to hold true for the Artemis astronauts. There is benefit in collecting the greatest diversity of samples possible with respect to grain size and composition. To broaden the potential science impact from returned samples, the Artemis astronauts should focus on material diversity and areas that may contain deeply excavated materials, among other activities and sampling related to the broader mission goals.

6 Concluding Remarks

The Artemis exploration zone contains several regions that may be explored by future crewed and uncrewed surface missions. Lithologies in this region were created from igneous and impact processes that have persisted over billions of years. Some brecciated samples may contain clasts petrogenetically unrelated to one another, which could be an efficient strategy to study a greater variety of lunar lithologies without venturing over large spatial regions on the surface. The potential for such breadth of lithological variety in an as-yet-unexplored region of the Moon will provide chronologic opportunities for untangling the mysterious history of lunar evolution. Chronologic opportunities that exist from analyses of returned samples include U-Th-P, Rb-Sr, Sm-Nd, Lu-Hf, and Ar-Ar.

These data will address issues such as the age of the Moon, timing of crucial events in lunar history, allow for recalibration of melt extraction model ages, crystallization ages of lithologies, and impact flux during the early Solar system. It is evident samples returned from the Artemis exploration zone will provide incredible insight into the history of the Moon and early Solar system. There is no 'silver bullet' analytical approach for all sample types. It will take a highly

coordinated effort between lithologies, chronometers, instruments, and institutions to fully understand what can be learned from these precious samples.

Acknowledgments

- The author acknowledges the Center for Lunar Science and Exploration for providing funding to support the completion of this manuscript.
- Since beginning this manuscript, the first author has become employed by Jacobs at NASA Johnson Space Center in addition to her doctoral studies at University of Houston.

Open Research

The reflectance and compositional mosaics used in this study are derived from Lemelin et al. (2022) and can be found in Zenodo:10.5281/zenodo.5847000.

References

Abelson P. H. (1970) The Moon Issue. *Science* **167**, 447–447.

Albee A. L., Chodos A. A., Dymek R. F., Gancarz A. J., Goldman D. S., Papanastassiou D. A. and Wasserburg G. J. (1974) Dunite From the Lunar Highlands: Petrography, Deformational History, Rb-Sr Age. In *Lunar and Planetary Science Conference* p. 3.

Amelin Y. (2005) Meteorite Phosphates Show Constant ^{176} Lu Decay Rate Since 4557 Million Years Ago. *Science* **310**, 839–841.

Amelin Y. and Zaitsev A. N. (2002) Precise geochronology of phoscorites and carbonatites:: The critical role of U-series disequilibrium in age interpretations. *Geochimica et Cosmochimica Acta* **66**, 2399–2419.

Anderson A. T., Crewe A. V., Goldsmith J. R., Moore P. B., Newton J. C., Olsen E. J., Smith J. V. and Wyllie P. J. (1970) Petrologic History of Moon Suggested by Petrography, Mineralogy, and Crystallography. *Science* **167**, 587–590.

Arvidson R. E., Boyce J., Chapman C., Cintala M., Fulchignoni M., Moore H., Neukum G., Schultz P. H., Soderblom L., Strom R., Woronow A. and Young R. (1979) Standard techniques for presentation and analysis of crater size-frequency data. *Icarus* **37**, 467–474.

Ballhaus C., Laurenz V., Münker C., Fonseca R. O. C., Albarède F., Rohrbach A., Lagos M., Schmidt M. W., Jochum K.-P., Stoll B., Weis U. and Helmy H. M. (2013) The U/Pb ratio of the Earth's mantle—A signature of late volatile addition. *Earth and Planetary Science Letters* **362**, 237–245.

Barboni Melanie, Boehnke P., Keller B., Kohl I. E., Schoene B., Young E. D. and McKeegan K. D. (2017) Early formation of the Moon 4.51 billion years ago. *Sci. Adv.* **3**, e1602365.

1058 Barboni M, Boehnke P., Keller C., Kohl I., Schoene B., Young E. and McKeegan K. (2017) The
1059 Age of the Moon. In id. 1900. Lunar and Planetary Science XLVIII. Lunar and Planetary
1060 Institute, The Woodlands, Texas.

1061 Barnes J. J., Kring D. A., Tartèse R., Franchi I. A., Anand M. and Russell S. S. (2016) An
1062 asteroidal origin for water in the Moon. *Nat Commun* **7**, 11684.

1063 Beard B. L., Taylor L. A., Scherer E. E., Johnson C. M. and Snyder G. A. (1998) The Source
1064 Region and Melting Mineralogy of High-Titanium and Low-Titanium Lunar Basalts
1065 Deduced from Lu-Hf Isotope Data. *Geochimica et Cosmochimica Acta* **62**, 525–544.

1066 Beard S. P., Swindle T. D., Lapen T. J. and Kring D. A. (2022) A r -A r and U - P b ages of
1067 Chelyabinsk and a re-evaluation of its impact chronology. *Meteorit & Planetary Scien*
1068 **57**, 2276–2288.

1069 Besserer J., Nimmo F., Wieczorek M. A., Weber R. C., Kiefer W. S., McGovern P. J., Andrews-
1070 Hanna J. C., Smith D. E. and Zuber M. T. (2014) GRAIL gravity constraints on the
1071 vertical and lateral density structure of the lunar crust. *Geophys. Res. Lett.* **41**, 5771–
1072 5777.

1073 Bickel V., Aaron J., Manconi A., Loew S. and Mall U. (2020) Impacts drive lunar rockfalls over
1074 billions of years. *Nature Communications* **11**.

1075 Bischoff A. and Stöffler D. (1984) Chemical and structural changes induced by thermal
1076 annealing of shocked feldspar inclusions in impact melt rocks from Lappajärvi Crater,
1077 Finland. *J. Geophys. Res.* **89**, B645.

1078 Bischoff A. and Stöffler D. (1992) Shock metamorphism as a fundamental process in the
1079 evolution of planetary bodies: Information from meteorites. *European Journal of*
1080 *Mineralogy* **4**, 707–755.

1081 Borg L., Connelly J., Boyet M. and Carlson R. (2011) The Age of Lunar Ferroan Anorthosite
1082 60025 with Implications for the Interpretation of Lunar Chronology and the Magma
1083 Ocean Model. In id. 1171. Lunar and Planetary Science XLII. Lunar and Planetary
1084 Institute, The Woodlands, Texas.

1085 Borg L. E., Brennecka G. A. and Kruijer T. S. (2022) The origin of volatile elements in the
1086 Earth–Moon system. *Proc. Natl. Acad. Sci. U.S.A.* **119**, e2115726119.

1087 Borg L. E. and Carlson R. W. (2023) The Evolving Chronology of Moon Formation. *Annu. Rev.*
1088 *Earth Planet. Sci.* **51**, annurev-earth-031621-060538.

1089 Borg L. E., Gaffney A. M., Kruijer T. S., Marks N. A., Sio C. K. and Wimpenny J. (2019)
1090 Isotopic evidence for a young lunar magma ocean. *Earth and Planetary Science Letters*
1091 **523**, 115706.

1092 Borg L. E., Gaffney A. M. and Shearer C. K. (2015) A review of lunar chronology revealing a
1093 preponderance of 4.34-4.37 Ga ages. *Meteorit Planet Sci* **50**, 715–732.

1094 Borg L. E., Gaffney A. M., Shearer C. K., DePaolo D. J., Hutcheon I. D., Owens T. L., Ramon
1095 E. and Brennecka G. (2009) Mechanisms for incompatible-element enrichment on the
1096 Moon deduced from the lunar basaltic meteorite Northwest Africa 032. *Geochimica et*
1097 *Cosmochimica Acta* **73**, 3963–3980.

1098 Borst A. M., Foing B. H., Davies G. R. and van Westrenen W. (2012) Surface mineralogy and
1099 stratigraphy of the lunar South Pole-Aitken basin determined from Clementine UV/VIS
1100 and NIR data. *Planetary and Space Science* **68**, 76–85.

1101 Bottke W. F., Walker R. J., Day J. M. D., Nesvorny D. and Elkins-Tanton L. (2010) Stochastic
1102 Late Accretion to Earth, the Moon, and Mars. *Science* **330**, 1527–1530.

1103 Boyce J. M., Schaber G. G. and Dial Jr A. L. (1977) Age of Luna 24 mare basalts based on crater
1104 studies. *Nature* **265**, 38–39.

1105 Boyet M. and Carlson R. W. (2007) A highly depleted moon or a non-magma ocean origin for
1106 the lunar crust? *Earth and Planetary Science Letters* **262**, 505–516.

1107 Brandon A. D., Lapen T. J., Debaille V., Beard B. L., Rankenburg K. and Neal C. (2009) Re-
1108 evaluating 142Nd/144Nd in lunar mare basalts with implications for the early evolution
1109 and bulk Sm/Nd of the Moon. *Geochimica et Cosmochimica Acta* **73**, 6421–6445.

1110 Brown H. M., Boyd A. K., Denevi B. W., Henriksen M. R., Manheim M. R., Robinson M. S.,
1111 Speyerer E. J. and Wagner R. V. (2022) Resource potential of lunar permanently
1112 shadowed regions. *Icarus* **377**, 114874.

1113 Burgess R., Fernandes V. A., Irving A. J. and Bunch T. E. (2007) Ar-Ar Ages of NWA 2977 and
1114 NWA 3160 – Lunar Meteorites Paired with NWA 773. In Lunar and Planetary Science
1115 XXXVIII. The Lunar and Planetary Science Institute, The Woodlands, Texas. p. Abstract
1116 1603.

1117 Bussey D. B. J., McGovern J. A., Spudis P. D., Neish C. D., Noda H., Ishihara Y. and Sørensen
1118 S.-A. (2010) Illumination conditions of the south pole of the Moon derived using Kaguya
1119 topography. *Icarus* **208**, 558–564.

1120 Cao H., Ling Z., Chen J., Fu X., Zou Y. and Joy K. (2021) Petrography, mineralogy, and
1121 geochemistry of a new lunar magnesian feldspathic meteorite Northwest Africa 11460.
1122 *Meteorit Planet Sci* **56**, 1857–1889.

1123 Carlson R. W., Borg L. E., Gaffney A. M. and Boyet M. (2014) Rb-Sr, Sm-Nd and Lu-Hf
1124 isotope systematics of the lunar Mg-suite: the age of the lunar crust and its relation to the
1125 time of Moon formation. *Phil. Trans. R. Soc. A.* **372**, 20130246.

1126 Černok A., White L. F., Anand M., Tait K. T., Darling J. R., Whitehouse M., Miljković K.,
1127 Lemelin M., Reddy S. M., Fougerouse D., Rickard W. D. A., Saxey D. W. and Ghent R.
1128 (2021) Lunar samples record an impact 4.2 billion years ago that may have formed the
1129 Serenitatis Basin. *Commun Earth Environ* **2**, 1–9.

1130 Charlier B. L. A., Ginibre C., Morgan D., Nowell G. M., Pearson D. G., Davidson J. P. and
1131 Ottley C. J. (2006) Methods for the microsampling and high-precision analysis of
1132 strontium and rubidium isotopes at single crystal scale for petrological and
1133 geochronological applications. *Chemical Geology* **232**, 114–133.

1134 Che X., Nemchin A., Liu D., Long T., Wang C., Norman M. D., Joy K. H., Tartese R., Head J.,
1135 Jolliff B., Snape J. F., Neal C. R., Whitehouse M. J., Crow C., Benedix G., Jourdan F.,
1136 Yang Z., Yang C., Liu J., Xie S., Bao Z., Fan R., Li D., Li Z. and Webb S. G. (2021) Age
1137 and composition of young basalts on the Moon, measured from samples returned by
1138 Chang'e-5. *Science* **374**, 887–890.

1139 Cheek L. C., Donaldson Hanna K. L., Pieters C. M., Head J. W. and Whitten J. L. (2013) The
1140 distribution and purity of anorthosite across the Orientale basin: New perspectives from
1141 Moon Mineralogy Mapper data: CRYSTALLINE ANORTHOSITE ACROSS
1142 ORIENTALE. *J. Geophys. Res. Planets* **118**, 1805–1820.

1143 Cherniak D. J. and Watson E. B. (2001) Pb diffusion in zircon. *Chemical Geology* **172**, 5–24.

1144 Chew D., Drost K., Marsh J. H. and Petrus J. A. (2021) LA-ICP-MS imaging in the geosciences
1145 and its applications to geochronology. *Chemical Geology* **559**, 119917.

1146 Coan D. (2020) Exploration EVA System Concept of Operations.

1147 Cohen B. A., Swindle T. D. and Kring D. A. (2005) Geochemistry and ^{40}Ar-^{39}Ar
1148 geochronology of impact-melt clasts in feldspathic lunar meteorites: Implications for
1149 lunar bombardment history. *Meteoritics & Planetary Science* **40**, 755–777.

1150 Cohen B. A., Swindle T. D. and Kring D. A. (2000) Support for the Lunar Cataclysm Hypothesis
1151 from Lunar Meteorite Impact Melt Ages. *Science* **290**, 1754–1756.

1152 Ćuk M., Gladman B. J. and Stewart S. T. (2010) Constraints on the source of lunar cataclysm
1153 impactors. *Icarus* **207**, 590–594.

1154 Culler T. S., Becker T. A., Muller R. A. and Renne P. R. (2000) Lunar Impact History from ^{40}
1155 Ar/ ^{39}Ar Dating of Glass Spherules. *Science* **287**, 1785–1788.

1156 Curran N. M., Joy K. H., Snape J. F., Pernet-Fisher J. F., Gilmour J. D., Nemchin A. A.,
1157 Whitehouse M. J. and Burgess R. (2019) The early geological history of the Moon
1158 inferred from ancient lunar meteorite Miller Range 13317. *Meteorit & Planetary Scien*
1159 **54**, 1401–1430.

1160 Dalrymple G. B. and Ryder G. (1993) ^{40}Ar/ ^{39}Ar age spectra of Apollo 15 impact melt rocks by
1161 laser step-heating and their bearing on the history of lunar basin formation. *J. Geophys.*
1162 *Res.* **98**, 13085–13095.

1163 Dalrymple G. B. and Ryder G. (1991) ^{40}AR/ ^{39}Ar ages of six Apollo 15 impact melt rocks by
1164 laser step heating. *Geophysical Research Letters* **18**, 1163–1166.

1165 Dalrymple G. B. and Ryder G. (1996) Argon-40/argon-39 age spectra of Apollo 17 highlands
1166 breccia samples by laser step heating and the age of the Serenitatis basin. *J. Geophys.*
1167 *Res.* **101**, 26069–26084.

1168 Dauphas N., Hopp T., Craig G., J. Zhang Z., C. Valdes M., R. Heck P., A. Charlier B. L., A. Bell
1169 E., Mark Harrison T., M. Davis A., Dussubieux L., R. Williams P., J. Krawczynski M.,
1170 Bouman C., S. Lloyd N., Tollstrup D. and B. Schwieters J. (2022) In situ 87 Rb– 87 Sr
1171 analyses of terrestrial and extraterrestrial samples by LA-MC-ICP-MS/MS with double
1172 Wien filter and collision cell technologies. *Journal of Analytical Atomic Spectrometry* **37**,
1173 2420–2441.

1174 Day J. M., Floss C., Taylor L. A., Anand M. and Patchen A. D. (2006) Evolved mare basalt
1175 magmatism, high Mg/Fe feldspathic crust, chondritic impactors, and the petrogenesis of
1176 Antarctic lunar breccia meteorites Meteorite Hills 01210 and Pecora Escarpment 02007.
1177 *Geochimica et Cosmochimica Acta* **70**, 5957–5989.

1178 Deutsch A. N., Head J. W. and Neumann G. A. (2020) Analyzing the ages of south polar craters
1179 on the Moon: Implications for the sources and evolution of surface water ice. *Icarus* **336**,
1180 113455.

1181 Deutsch A. and Scharer U. (1994) Dating terrestrial impact events. *Meteoritics* **29**, 301–322.

1182 Deutsch A. and Stöffler D. (1987) Rb-Sr-analyses of Apollo 16 melt rocks and a new age
1183 estimate for the Imbrium basin: Lunar basin chronology and the early heavy
1184 bombardment of the moon. *Geochimica et Cosmochimica Acta* **51**, 1951–1964.

1185 Donaldson Hanna K. L., Cheek L. C., Pieters C. M., Mustard J. F., Greenhagen B. T., Thomas I.
1186 R. and Bowles N. E. (2014) Global assessment of pure crystalline plagioclase across the
1187 Moon and implications for the evolution of the primary crust: Pure Plagioclase on the
1188 Moon. *J. Geophys. Res. Planets* **119**, 1516–1545.

1189 Dressler B. O. and Reimold W. U. (2001) Terrestrial impact melt rocks and glasses. *Earth-*
1190 *Science Reviews* **56**, 205–284.

1191 Duncan A. R., Mckay S. M., Stoeser J. W., Lindstrom M. M., Lindstrom D. J., Fruchter J. S. and
1192 Goles G. G. (1975) Lunar polymict breccia 14321: a compositional study of its principal
1193 components. *Geochimica et Cosmochimica Acta* **39**, 247–260.

1194 Dymek R. F., Albee A. L. and Chodos A. A. (1975) Comparative petrology of lunar cumulate
1195 rocks of possible primary origin: dunite 72415, troctolite 76535, norite 78235, and
1196 anorthosite 62237. In Lunar Science Conference VI. New York, Pergamon Press, Inc.,
1197 Houston, Texas. pp. 301–341.

1198 Edmunson J., Borg L. E., Nyquist L. E. and Asmerom Y. (2009) A combined Sm–Nd, Rb–Sr,
1199 and U–Pb isotopic study of Mg-suite norite 78238: Further evidence for early
1200 differentiation of the Moon. *Geochimica et Cosmochimica Acta* **73**, 514–527.

1201 Elardo S. M., Draper D. S. and Shearer C. K. (2011) Lunar Magma Ocean crystallization
1202 revisited: Bulk composition, early cumulate mineralogy, and the source regions of the
1203 highlands Mg-suite. *Geochimica et Cosmochimica Acta* **75**, 3024–3045.

1204 Elardo S. M., McCubbin F. M. and Shearer C. K. (2012) Chromite symplectites in Mg-suite
1205 troctolite 76535 as evidence for infiltration metasomatism of a lunar layered intrusion.
1206 *Geochimica et Cosmochimica Acta* **87**, 154–177.

1207 Elkins-Tanton L. T., Burgess S. and Yin Q.-Z. (2011) The lunar magma ocean: Reconciling the
1208 solidification process with lunar petrology and geochronology. *Earth and Planetary*
1209 *Science Letters* **304**, 326–336.

1210 Elkins-Tanton L. T., Van Orman J. A., Hager B. H. and Grove T. L. (2002) Re-examination of
1211 the lunar magma ocean cumulate overturn hypothesis: melting or mixing is required.
1212 *Earth and Planetary Science Letters* **196**, 239–249.

1213 Eugster O., Geiss J. and Grogler N. (1983) Dating of early regolith exposure and the evolution of
1214 trapped 40Ar/36Ar with time. *14th Lunar and Planetary Science Conference*, 177–178.

1215 Eugster O., Groegler N., Eberhardt P. and Geiss J. (1980) Double drive tube 74001/2-
1216 Composition of noble gases trapped 3.7 AE ago. In In: Lunar and Planetary Science
1217 Conference, 11th, Houston, TX, March 17-21, 1980, Proceedings. Volume 2.(A82-22296
1218 09-91) New York, Pergamon Press, 1980, p. 1565-1592. Swiss National Science
1219 Foundation. pp. 1565–1592.

1220 Eugster O. and Polnau E. (1997) Further data for the calibration of the antiquity indicator Ar-
1221 40/Ar-36 for lunar soil. In Conference Paper, 28th Annual Lunar and Planetary Science
1222 Conference, p. 341. p. 341.

1223 Eugster O., Terribilini D., Polnau E. and Kramers J. (2001) The antiquity indicator argon-
1224 40/argon-36 for lunar surface samples calibrated by uranium-235-xenon-136 dating.
1225 *Meteoritics & Planetary Science* **36**, 1097–1115.

1226 Fagan A. L., Joy K. H., Bogard D. D. and Kring D. A. (2014) Ages of Globally Distributed
1227 Lunar Paleoregoliths and Soils from 3.9 Ga to the Present. *Earth Moon Planets* **112**, 59–
1228 71.

1229 Fairweather J. H., Lagain A., Servis K., Benedix G. K., Kumar S. S. and Bland P. A. (2022)
1230 Automatic Mapping of Small Lunar Impact Craters Using LRO-NAC Images. *Earth and*
1231 *Space Science* **9**.

1232 Fernandes V. A., Fritz J., Weiss B. P., Garrick-Bethell I. and Shuster D. L. (2013) The
1233 bombardment history of the Moon as recorded by ^{40} Ar- ^{39} Ar chronology. *Meteorit*
1234 *Planet Sci* **48**, 241–269.

1235 Gaffney A. M. and Borg L. E. (2014) A young solidification age for the lunar magma ocean.
1236 *Geochimica et Cosmochimica Acta* **140**, 227–240.

1237 Gagnepain-Beyneix J., Lognonné P., Chenet H., Lombardi D. and Spohn T. (2006) A seismic
1238 model of the lunar mantle and constraints on temperature and mineralogy. *Physics of the*
1239 *Earth and Planetary Interiors* **159**, 140–166.

1240 Ganapathy R., Morgan J., Higuchi H., Anders E. and Anderson Jr A. (1974) Meteoritic and
1241 volatile elements in Apollo 16 rocks and in separated phases from 14306 Lunar Science
1242 V. *The Lunar Science Institute. Part*, 257–259.

1243 Garrick-Bethell I., Miljković K., Hiesinger H., van der Bogert C. H., Laneuville M., Shuster D.
1244 L. and Korycansky D. G. (2020) Troctolite 76535: A sample of the Moon's South Pole-
1245 Aitken basin? *Icarus* **338**, 113430.

1246 Garrick-Bethell I. and Zuber M. T. (2009) Elliptical structure of the lunar South Pole-Aitken
1247 basin. *Icarus* **204**, 399–408.

1248 Gawronska A. J., Barrett N., Boazman S. J., Gilmour C. M., Halim S. H., Harish, McCanaan K.,
1249 Satyakumar A. V., Shah J., Meyer H. M. and Kring D. A. (2020) Geologic context and
1250 potential EVA targets at the lunar south pole. *Advances in Space Research* **66**, 1247–
1251 1264.

1252 Gopalan K., Kaushal S., Lee-Hu C. and Wetherill G. (1970) Rb-Sr and U, Th-Pb ages of lunar
1253 materials. *Geochimica et Cosmochimica Acta Supplement* **2**, 1195–1205.

1254 Grieve R. A. F., Stöffler D. and Deutsch A. (1991) The Sudbury structure: Controversial or
1255 misunderstood? *J. Geophys. Res.* **96**, 22753.

1256 Grieve R. A., McKay G. A., Smith H. D. and Weill D. F. (1975) Lunar polymict breccia 14321:
1257 a petrographic study. *Geochimica et Cosmochimica Acta* **39**, 229–245.

1258 Gros J., Takahashi H., Hertogen J., Morgan J. W. and Anders E. (1976) Composition of the
1259 projectiles that bombarded the lunar highlands. In In: Lunar Science Conference, 7th,
1260 Houston, Tex., March 15-19, 1976, Proceedings. Volume 2.(A77-34651 15-91) New
1261 York, Pergamon Press, Inc., 1976, p. 2403-2425. pp. 2403–2425.

1262 Gross J., Hilton A., Prissel T. C., Setera J. B., Korotev R. L. and Calzada-Diaz A. (2020)
1263 Geochemistry and Petrogenesis of Northwest Africa 10401: A New Type of the Mg-Suite
1264 Rocks. *JGR Planets* **125**.

1265 Gross J., Treiman A. H. and Mercer C. N. (2014) Lunar feldspathic meteorites: Constraints on
1266 the geology of the lunar highlands, and the origin of the lunar crust. *Earth and Planetary*
1267 *Science Letters* **388**, 318–328.

1268 Halim S., Barrett N., Boazman S., Gawronska A., Gilmour C., Harish, McCanaan K.,
1269 Satyakumar A., Shah J. and Kring D. (2021) Numerical modeling of the formation of
1270 Shackleton crater at the lunar south pole. *Icarus* **354**, 113992.

1271 Hapke B. (1981) Bidirectional reflectance spectroscopy: 1. Theory. *J. Geophys. Res.* **86**, 3039–
1272 3054.

1273 Hapke B. (2001) Space weathering from Mercury to the asteroid belt. *J. Geophys. Res.* **106**,
1274 10039–10073.

1275 Haruyama J., Matsunaga T., Ohtake M., Morota T., Honda C., Yokota Y., Torii M., Ogawa Y.,
1276 and LISM Working Group (2008) Global lunar-surface mapping experiment using the
1277 Lunar Imager/Spectrometer on SELENE. *Earth, Planets and Space* **60**, 243–255.

1278 Haskin L. A. (1998) The Imbrium impact event and the thorium distribution at the lunar
1279 highlands surface. *J. Geophys. Res.* **103**, 1679–1689.

1280 Haskin L. A., Korotev R. L., Rockow K. M. and Jolliff B. L. (1998) The case for an Imbrium
1281 origin of the Apollo thorium-rich impact-melt breccias. *Meteoritics & Planetary Science*
1282 **33**, 959–975.

1283 Hawke B. R. (2003) Distribution and modes of occurrence of lunar anorthosite. *J. Geophys. Res.*
1284 **108**, 5050.

1285 Head J. W., Murchie S., Mustard J. F., Pieters C. M., Neukum G., McEwen A., Greeley R.,
1286 Nagel E. and Belton M. J. S. (1993) Lunar impact basins: New data for the western limb
1287 and far side (Orientale and South Pole-Aitken Basins) from the first Galileo flyby. *J.*
1288 *Geophys. Res.* **98**, 17149.

1289 Head J. W. and Wilson L. (1992) Lunar mare volcanism: Stratigraphy, eruption conditions, and
1290 the evolution of secondary crusts. *Geochimica et Cosmochimica Acta* **56**, 2155–2175.

1291 Hess P. C. (1994) Petrogenesis of lunar troctolites. *J. Geophys. Res.* **99**, 19083.

1292 Hess P. C. and Parmentier E. M. (1995) A model for the thermal and chemical evolution of the
1293 Moon's interior: implications for the onset of mare volcanism. *Earth and Planetary*
1294 *Science Letters* **134**, 501–514.

1295 Hiesinger H. (2006) New Views of Lunar Geoscience: An Introduction and Overview. *Reviews*
1296 *in Mineralogy and Geochemistry* **60**, 1–81.

1297 Hiesinger H., van der Bogert C. H., Pasckert J. H., Funcke L., Giacomini L., Ostrach L. R. and
1298 Robinson M. S. (2012) How old are young lunar craters? *Journal of Geophysical*
1299 *Research: Planets* **117**.

1300 Higuchi H. and Morgan J. W. (1975) Ancient meteoritic component in Apollo 17 boulders. In
1301 Lunar and Planetary Science Conference Proceedings. pp. 1625–1651.

1302 Horz F., Grieve R., Heiken G., Spudis P. and Binder A. (1991) Chapter 4: Lunar Surface
1303 Processes. In *The Lunar Sourcebook* Cambridge University Press/Lunar and Planetary
1304 Institute. pp. 61–120.

1305 Howard K. A., Wilhelms D. E. and Scott D. H. (1974) Lunar basin formation and highland
1306 stratigraphy. *Rev. Geophys.* **12**, 309.

Huang (**黄俊**) J., Xiao (**肖智勇**) Z., Xiao (**肖**龙) L., Horgan B., Hu (**胡**晓依) X., Lucey P., Xiao (**肖**潇) X., Zhao (赵思源) S., Qian (钱煜奇) Y., Zhang (张昊) H., Li (**李春来**) C., Xu (**徐**睿) R., He (**何志平**) Z., Yang (杨建峰) J., Xue (**薛彬**) B., He (**何琦**) Q., Zhong (钟杰) J., Lin (**林宏宇**) H., Huang (**黄**长宁) C. and Xie (谢剑锋) J. (2020) Diverse rock types detected in the lunar South Pole–Aitken Basin by the Chang'E-4 lunar mission. *Geology* **48**, 723–727.

Hui H., Neal C. R., Shih C.-Y. and Nyquist L. E. (2013) Petrogenetic association of the oldest lunar basalts: Combined Rb–Sr isotopic and trace element constraints. *Earth and Planetary Science Letters* **373**, 150–159.

Hult M., Vidmar T., Rosengård U., Marissens G., Lutter G. and Sahin N. (2014) Half-life measurements of lutetium-176 using underground HPGe-detectors. *Applied Radiation and Isotopes* **87**, 112–117.

Huneke J. C. (1978) 40Ar-39Ar Microanalysis of single 74220 glass balls and 72435 breccia clasts. *Proceedings of the Lunar and Planetary Science Conference* **9**, 2345–2362.

Hurley P. and Pinson, Jr. W. (1970) Whole-rock Rb-Sr isotopic age relationships in Apollo 11 lunar samples. *Geochimica et Cosmochimica Acta Supplement* **2**, 1195–1205.

Hurwitz D. M. and Kring D. A. (2014) Differentiation of the South Pole–Aitken basin impact melt sheet: Implications for lunar exploration. *J. Geophys. Res. Planets* **119**, 1110–1133.

Ibanez-Mejia M., Gehrels G. E., Ruiz J., Vervoort J. D., Eddy M. P. and Li C. (2014) Small-volume baddeleyite (ZrO2) U–Pb geochronology and Lu–Hf isotope geochemistry by LA-ICP-MS. Techniques and applications. *Chemical Geology* **384**, 149–167.

Jaffey A. H., Flynn K. F., Glendenin L. E., Bentley W. C. and Essling A. M. (1971) Precision Measurement of Half-Lives and Specific Activities of U 235 and U 238. *Phys. Rev. C* **4**, 1889–1906.

James O. (1996) Siderophile elements in lunar impact melts define nature of the impactors. In Lunar and Planetary Science, volume 27, page 603.

James O. B. (2002) Distinctive Meteoritic Components in Lunar``Cataclysm''Impact-Melt Breccias. In Lunar and Planetary Science Conference. p. 1210.

Johnston S., Brandon A., McLeod C., Rankenburg K., Becker H. and Copeland P. (2022) Nd isotope variation between the Earth–Moon system and enstatite chondrites. *Nature* **611**, 501–506.

Jolliff B. L., Gillis J. J., Haskin L. A., Korotev R. L. and Wieczorek M. A. (2000) Major lunar crustal terranes: Surface expressions and crust-mantle origins. *J. Geophys. Res.* **105**, 4197–4216.

1341 Jolliff B. L., Korotev R. L. and Haskin L. A. (1993) An iridium-rich iron micrometeorite with
1342 silicate inclusions from the Moon. In Lunar and Planetary Inst., Twenty-Fourth Lunar
1343 and Planetary Science Conference. Part 2: GM.

1344 Jourdan F. (2012) The 40Ar/39Ar dating technique applied to planetary sciences and terrestrial
1345 impacts. *Australian Journal of Earth Sciences* **59**, 199–224.

1346 Joy K. H., Crawford I. A., Anand M., Greenwood R. C., Franchi I. A. and Russell S. S. (2008)
1347 The petrology and geochemistry of Miller Range 05035: A new lunar gabbroic meteorite.
1348 *Geochimica et Cosmochimica Acta* **72**, 3822–3844.

1349 Joy K. H., Crawford I. A., Curran N. M., Zolensky M., Fagan A. F. and Kring D. A. (2016) The
1350 Moon: An Archive of Small Body Migration in the Solar System. *Earth Moon Planets*
1351 **118**, 133–158.

1352 Joy K. H., Kring D. A., Bogard D. D., McKay D. S. and Zolensky M. E. (2011) Re-examination
1353 of the formation ages of the Apollo 16 regolith breccias. *Geochimica et Cosmochimica*
1354 *Acta* **75**, 7208–7225.

1355 Joy K. H., Tartèse R., Messenger S., Zolensky M. E., Marrocchi Y., Frank D. R. and Kring D. A.
1356 (2020) The isotopic composition of volatiles in the unique Bench Crater carbonaceous
1357 chondrite impactor found in the Apollo 12 regolith. *Earth and Planetary Science Letters*
1358 **540**, 116265.

1359 Kenkmann T. and Artemieva N. (2021) The terrestrial impact crater record: A statistical analysis
1360 of morphologies, structures, ages, lithologies, and more. *Meteorit Planet Sci* **56**, 1024–
1361 1070.

1362 Kereszturi A., Tomka R., Gläser P. A., Pal B. D., Steinmann V. and Warren T. (2022)
1363 Characteristics of de Gerlache crater, site of girlands and slope exposed ice in a lunar
1364 polar depression. *Icarus* **388**, 115231.

1365 Kettrup B., Deutsch A. and Masaitis V. L. (2003) Homogeneous impact melts produced by a
1366 heterogeneous target? *Geochimica et Cosmochimica Acta* **67**, 733–750.

1367 Korotev R. L., Gillis J. J., Haskin L. A. and Jolliff B. L. (2002) On the Age of the Nectaris
1368 Basin. In The Moon Beyond 2002: Next Steps in Lunar Science and Exploration. p. 31.

1369 Kraettli G., Schmidt M. W. and Liebske C. (2022) Fractional crystallization of a basal lunar
1370 magma ocean: A dense melt-bearing garnetite layer above the core? *Icarus* **371**, 114699.

1371 Kramer G. Y., Kring D. A., Nahm A. L. and Pieters C. M. (2013) Spectral and photogeologic
1372 mapping of Schrödinger Basin and implications for post-South Pole-Aitken impact deep
1373 subsurface stratigraphy. *Icarus* **223**, 131–148.

1374 Krasilnikov S. S., Ivanov M. A., Head J. W. and Krasilnikov A. S. (2023) Geologic history of
1375 the south circumpolar region (SCR) of the Moon. *Icarus* **394**, 115422.

Kring D. A. (2008) Deciphering the Chronology and Implications of Impact Cratering on the Moon: A High Science Priority for Lunar Exploration. In Lunar and Planetary Science XXXIX. The Woodlands, TX.

Kring D. A. (2006) Exploring Lunar Impact Craters and Their Implications for the Origin and Early Evolution of Life on Earth.

Kring D. A. (2005) Hypervelocity collisions into continental crust composed of sediments and an underlying crystalline basement: comparing the Ries (~24 km) and Chicxulub (~180 km) impact craters. *Geochemistry* **65**, 1–46.

Kring D. A. (2019) Lunar South Pole Geology: Preparing for a Seventh Lunar Landing. In NASA Exploration Science Forum.

Kring D. A. (2009) Targeting Complex Craters and Multi-Ring Basins to Determine the Tempo of Impact Bombardment while Simultaneously Probing the Lunar Interior. In Lunar Reconnaissance Orbiter Science Targeting Meeting.

Kring D. A. (2007) Using the Moon to Determine the Magnitude of the Inner Solar System Cataclysm and Post-Cataclysm Impact Flux. In NAC Lunar Meeting.

Kring D. A., Bickel V. T., Van Der Bogert C. H., Fagan A. L., Gaddis L. R., Hiesinger H., Hurtado J. M., Joy K. H., Lemelin M., Looper C. A., Osinski G. R., Pösges G., Siegler M., Tikoo S. M. and Zacny K. (2023) Elevation Changes and Slope that May Affect EVA Workload Near Potential Artemis Landing Sites. In *2023 IEEE Aerospace Conference* 2023 IEEE Aerospace Conference. IEEE, Big Sky, MT, USA. pp. 1–17.

Kring D. A., Claeys P., Gulick S. P. S., Morgan J. V. and Collins G. S. (2017) Chicxulub and the Exploration of Large Peak-Ring Impact Craters through Scientific Drilling. *GSAT*, 4–8.

Kring D. A. and Cohen B. A. (2002) Cataclysmic bombardment throughout the inner solar system 3.9–4.0 Ga. *J. Geophys. Res.* **107**.

Kring D. A., Gruener J. E. and Eppler D. B. (2020) Artemis III EVA Opportunities on Malapert and Leibnitz B Massifs. *Science Definition Team for Artemis*.

Kring D. A., Kramer G. Y., Bussey D. B. J., Hurley D. M., Stickle A. M. and van der Bogert C. H. (2021) Prominent volcanic source of volatiles in the south polar region of the Moon. *Advances in Space Research* **68**, 4691–4701.

Kring D. A., Kramer G. Y., Collins G. S., Potter R. W. K. and Chandnani M. (2016) Peak-ring structure and kinematics from a multi-disciplinary study of the Schrödinger impact basin. *Nat Commun* **7**, 13161.

Kring D. A., Lemelin M., van der Bogert C. H., Bickel V., Hiesinger H., Hurtado J. M., Petro N., Siegler M. A., Looper C. A., Huning T., Osinski G. R. and Gaddis L. (2022) Geological EVA Science along a South Pole-Aitken (SPA) Basin Massif Ridge Cross-Cut by Shackleton Crater. In Lunar and Planetary Science LIII. The Woodlands, Texas.

Kring D. A., Swindle T. D., Strom R. G., Ito T. and Yoshida F. (2005) Exploring Impact Cratering on the Moon and its Implications for the Biologic Evolution of, and Habitable Conditions on, the Earth. In Space Resources Roundtable VII. Golden, Colorado.

Kruijer T. S. and Kleine T. (2017) Tungsten isotopes and the origin of the Moon. *Earth and Planetary Science Letters* **475**, 15–24.

Kumari N., Bretzfelder J. M., Ganesh I., Lang A. and Kring D. A. (2022) Surface Conditions and Resource Accessibility at Potential Artemis Landing Sites 007 and 011. *Planet. Sci. J.* **3**, 224.

Lagain A., Kreslavsky M., Baratoux D., Liu Y., Devillepoix H., Bland P., Benedix G. K., Doucet L. S. and Servis K. (2022) Has the impact flux of small and large asteroids varied through time on Mars, the Earth and the Moon? *Earth and Planetary Science Letters* **579**, 117362.

Lally J. S., Christie J. M., Nord Jr. G. L. and Heuer A. H. (1976) Deformation, recovery and recrystallization of lunar dunite 72417. In *Lunar and Planetary Science VII* New York, Pergamon Press, Inc., Houston, Texas. pp. 1845–1863.

Lapen T. J., Righter M., Brandon A. D., Debaille V., Beard B. L., Shafer J. T. and Peslier A. H. (2010) A Younger Age for ALH84001 and Its Geochemical Link to Shergottite Sources in Mars. *Science* **328**, 347–351.

Le Feuvre M. and Wieczorek M. A. (2011) Nonuniform cratering of the Moon and a revised crater chronology of the inner Solar System. *Icarus* **214**, 1–20.

Lemelin M., Lucey P. G. and Camon A. (2022) Compositional Maps of the Lunar Polar Regions Derived from the Kaguya Spectral Profiler and the Lunar Orbiter Laser Altimeter Data. *Planet. Sci. J.* **3**, 63.

Lemelin M., Lucey P. G., Crites S. T. and Jha K. (2017) Mineralogy and Iron Content of the Lunar Polar Regions using the Kaguya Spectral Profiler and the Lunar Orbiter Laser Altimeter. In *New Views of the Moon 2* Europe.

Lemelin M., Lucey P. G., Miljković K., Gaddis L. R., Hare T. and Ohtake M. (2019) The compositions of the lunar crust and upper mantle: Spectral analysis of the inner rings of lunar impact basins. *Planetary and Space Science* **165**, 230–243.

Lemelin M., Lucey P. G., Song E. and Taylor G. J. (2015) Lunar central peak mineralogy and iron content using the Kaguya Multiband Imager: Reassessment of the compositional structure of the lunar crust: LUNAR CENTRAL PEAK MINERALOGY AND IRON. *J. Geophys. Res. Planets* **120**, 869–887.

Levinson A. A. (1970) Proceedings of the Apollo 11 Lunar Science Conference (issued as Geochimica et Cosmochimica Acta, supplement no. 1, vol. 34, 1970). *Geochimica et Cosmochimica Acta* **34**, 1367–1372.

Li Q.-L., Zhou Q., Liu Y., Xiao Z., Lin Y., Li J.-H., Ma H.-X., Tang G.-Q., Guo S., Tang X., Yuan J.-Y., Li J., Wu F.-Y., Ouyang Z., Li C. and Li X.-H. (2021) Two-billion-year-old volcanism on the Moon from Chang'e-5 basalts. *Nature* **600**, 54–58.

Li S. and Milliken R. E. (2017) Water on the surface of the Moon as seen by the Moon Mineralogy Mapper: Distribution, abundance, and origins. *Sci. Adv.* **3**, e1701471.

Lin Honglei, He Z., Yang W., Lin Y., Xu R., Zhang C., Zhu M.-H., Chang R., Zhang J., Li C., Lin Hongyu, Liu Y., Gou S., Wei Y., Hu S., Xue C., Yang J., Zhong J., Fu X., Wan W. and Zou Y. (2020) Olivine-norite rock detected by the lunar rover Yutu-2 likely crystallized from the SPA impact melt pool. *National Science Review* **7**, 913–920.

Lock S. J., Stewart S. T., Petaev M. I., Leinhardt Z., Mace M. T., Jacobsen S. B. and Cuk M. (2018) The Origin of the Moon Within a Terrestrial Synestia. *J. Geophys. Res. Planets* **123**, 910–951.

Lovering J. F., Wark D. A., Gleadow A. J. W. and Britten R. (1974) Lunar monazite: A late-stage (mesostasis) phase in mare basalt. *Earth and Planetary Science Letters* **21**, 164–168.

Lucey P. G., Taylor G. J., Hawke B. R. and Spudis P. D. (1998) FeO and TiO_2 concentrations in the South Pole-Aitken basin: Implications for mantle composition and basin formation. *J. Geophys. Res.* **103**, 3701–3708.

Lucey P., Korotev R., Gillis J., Taylor L., Lawrence D., Campbell B., Elphic R., Feldman B., Hood L., Hunten D., Mendillo M., Noble S., Papike J., Reedy R., Lawson S., Prettyman T., Gasnault O. and Maurice S. (2006) Understanding the Lunar Surface and Space-Moon Interactions. In *Reviews in Mineralogy and Geochemistry* Mineralogical Society of America. pp. 83–219.

Marks N. E., Borg L. E., Shearer C. K. and Cassata W. S. (2019) Geochronology of an Apollo 16 Clast Provides Evidence for a Basin-Forming Impact 4.3 Billion Years Ago. *JGR Planets* **124**, 2465–2481.

Mazarico E., Neumann G. A., Smith D. E., Zuber M. T. and Torrence M. H. (2011) Illumination conditions of the lunar polar regions using LOLA topography. *Icarus* **211**, 1066–1081.

Mazrouei S., Ghent R. R., Bottke W. F., Parker A. H. and Gernon T. M. (2019) Earth and Moon impact flux increased at the end of the Paleozoic. *Science* **363**, 253–257.

McCallum I. S., Domeneghetti M. C., Schwartz J. M., Mullen E. K., Zema M., Cámara F., McCammon C. and Ganguly J. (2006) Cooling history of lunar Mg-suite gabbronorite 76255, troctolite 76535 and Stillwater pyroxenite SC-936: The record in exsolution and ordering in pyroxenes. *Geochimica et Cosmochimica Acta* **70**, 6068–6078.

McCubbin F. M. and Barnes J. J. (2020) The chlorine-isotopic composition of lunar KREEP from magnesian-suite troctolite 76535. *American Mineralogist* **105**, 1270–1274.

McDougall I., Harrison T. M., McDougall P. of G. I. and Harrison P. of G. D. of E. and S. S. T. M. (1999) *Geochronology and Thermochronology by the 40Ar/39Ar Method*., Oxford University Press.

McKay D. S., Bogard D. D., Morris R. V., Korotev R. L., Johnson P. and Wentworth S. J. (1986) Apollo 16 regolith breccias: Characterization and evidence for early formation in the mega-regolith. *J. Geophys. Res.* **91**, 277–303.

McKay D. S., Heiken G., Basu A., Blanford G., Simon S., Reedy R., French B. M. and Papike J. (1991) Chapter 7: The Lunar Regolith. In *The Lunar Sourcebook* Cambridge University Press/Lunar and Planetary Institute. pp. 285–356.

McLeod C. L., Brandon A. D. and Armytage R. M. G. (2014) Constraints on the formation age and evolution of the Moon from 142Nd–143Nd systematics of Apollo 12 basalts. *Earth and Planetary Science Letters* **396**, 179–189.

McLeod C. L., Brandon A. D., Fernandes V. A., Peslier A. H., Fritz J., Lapen T., Shafer J. T., Butcher A. R. and Irving A. J. (2016) Constraints on formation and evolution of the lunar crust from feldspathic granulitic breccias NWA 3163 and 4881. *Geochimica et Cosmochimica Acta* **187**, 350–374.

McSween Jr H. Y. (1976) A new type of chondritic meteorite found in lunar soil. *Earth and Planetary Science Letters* **31**, 193–199.

Mercer C. M. and Hodges K. V. (2016) ArAR — A software tool to promote the robust comparison of K–Ar and 40Ar/39Ar dates published using different decay, isotopic, and monitor-age parameters. *Chemical Geology* **440**, 148–163.

Mercer C. M., Hodges K. V., Jolliff B. L., Van Soest M. C., Wartho J. and Weirich J. R. (2019) Exploring the variability of argon loss in Apollo 17 impact melt rock 77135 using high-spatial resolution ^{40} Ar/ ^{39} Ar geochronology. *Meteorit & Planetary Scien* **54**, 721–739.

Mercer C. M., Young K. E., Weirich J. R., Hodges K. V., Jolliff B. L., Wartho J.-A. and Van Soest M. C. (2015) Refining lunar impact chronology through high spatial resolution ^{40} Ar/ ^{39} Ar dating of impact melts. *Sci. Adv.* **1**, e1400050.

Merle R. E., Nemchin A. A., Grange M. L., Whitehouse M. J. and Pidgeon R. T. (2014) High resolution U-Pb ages of Ca-phosphates in Apollo 14 breccias: Implications for the age of the Imbrium impact. *Meteorit Planet Sci* **49**, 2241–2251.

Meyer H. M., Denevi B. W., Boyd A. K. and Robinson M. S. (2016) The distribution and origin of lunar light plains around Orientale basin. *Icarus* **273**, 135–145.

Michaut C. and Pinel V. (2018) Magma Ascent and Eruption Triggered by Cratering on the Moon: MAGMA ASCENT BELOW IMPACT CRATERS. *Geophys. Res. Lett.* **45**, 6408–6416.

1519 Miljković K., Wieczorek M. A., Laneuville M., Nemchin A., Bland P. A. and Zuber M. T.
1520 (2021) Large impact cratering during lunar magma ocean solidification. *Nat Commun* **12**,
1521 5433.

1522 Moore H. J., Hodges C. A. and Scott D. H. (1974) Multiringed basins- illustrated by Orientale
1523 and associated features. In *Proceedings of the Lunar and Planetary Science, V*
1524 Supplement 5, Geochimica et Cosmochimica Acta. Pergamon Press Inc., Houston, Texas.
1525 pp. 71–100.

1526 Morbidelli A., Marchi S., Bottke W. F. and Kring D. A. (2012) A sawtooth-like timeline for the
1527 first billion years of lunar bombardment. *Earth and Planetary Science Letters* **355–356**,
1528 144–151.

1529 Morgan J. W., Krahenbuhl U., Ganapathy R. and Anders E. (1972a) Trace elements in Apollo 15
1530 samples: implications for meteorite influx and volatile depletion on the moon.
1531 *Proceedings of the Third Lunar Science Conference* **2**, 1361–1376.

1532 Morgan J. W., Laul J. C., Krahenbuhl U., Ganapathy R. and Anders E. (1972b) Major impacts on
1533 the Moon: characterizationfrom trace elements in Apollo 12 and 14 samples. *Proceedings*
1534 *of the Third Lunar Science Conference* **3**, 1377.

1535 Moriarty Daniel P., Dygert N., Valencia S. N., Watkins R. N. and Petro N. E. (2021) The search
1536 for lunar mantle rocks exposed on the surface of the Moon. *Nat Commun* **12**, 4659.

1537 Moriarty D. P. and Pieters C. M. (2018) The Character of South Pole-Aitken Basin: Patterns of
1538 Surface and Subsurface Composition. *J. Geophys. Res. Planets* **123**, 729–747.

1539 Moriarty D. P., Watkins R. N., Valencia S. N., Kendall J. D., Evans A. J., Dygert N. and Petro N.
1540 E. (2021) Evidence for a Stratified Upper Mantle Preserved Within the South Pole-
1541 Aitken Basin. *J Geophys Res Planets* **126**.

1542 Mukhametshin Ch. R., Semenov A. and Shpekin M. (2018) Experience of modeling relief of
1543 impact lunar crater Aitken based on high-resolution orbital images. *Journal of Physics:*
1544 *Conference Series* **1015**.

1545 Müller W. F. and Hornemann U. (1969) Shock-induced planar deformation structures in
1546 experimentally shock-loaded olivines and in olivines from chondritic meteorites. *Earth*
1547 *and Planetary Science Letters* **7**, 251–264.

1548 Nagaoka H., Takeda H., Karouji Y., Ohtake M., Yamaguchi A., Yoneda S. and Hasebe N.
1549 (2014) Implications for the origins of pure anorthosites found in the feldspathic lunar
1550 meteorites, Dhofar 489 group. *Earth, Planets and Space* **66**, 115.

1551 Nagurney A. B., Treiman A. H. and Spudis P. D. (2016) Petrology, Bulk Composition, and
1552 Provenance of Meteorite Northwest Africa 5000 (NWA 5000). In 47th Lunar and
1553 Planetary Science Conference. The Woodlands, TX.

Nakamura R., Matsunaga T., Ogawa Y., Yamamoto S., Hiroi T., Saiki K., Hirata N., Arai T., Kitazato K., Takeda H., Sugihara T., Kodama S., Ohtake M., Haruyama J. and Yokota Y. (2009) Ultramafic impact melt sheet beneath the South Pole–Aitken basin on the Moon. *Geophys. Res. Lett.* **36**, L22202.

NASA (2022) NASA Identifies Candidate Regions for Landing Next Americans on Moon. *NASA*.

NASA (2021) NASA Prompts Companies for Artemis Lunar Terrain Vehicle Solutions. *Press Release*.

NASA (2023) NASA Pursues Lunar Terrain Vehicle Services for Artemis Missions. *Press Release*.

NASA (2020a) NASA's lunar exploration program overview. *NASA's lunar exploration program overview*.

NASA (2020b) *NASA's Plan for Sustained Lunar Exploration and Development*., National Aeronautics and Space Administration.

Nelson W. S., Hammer J. E., Shea T., Hellebrand E. and Jeffrey Taylor G. (2021) Chemical heterogeneities reveal early rapid cooling of Apollo Troctolite 76535. *Nat Commun* **12**, 7054.

Nemchin A., Timms N., Pidgeon R., Geisler T., Reddy S. and Meyer C. (2009) Timing of crystallization of the lunar magma ocean constrained by the oldest zircon. *Nature Geosci* **2**, 133–136.

Neukum G. (1984) *Meteorite bombardment and dating of planetary surfaces, Translation of: Meteoritenbombardement und Datierung planetarer Oberflächen, Tenure Thesis, Ludwig-Maximilians University, Munich, Germany*., NASA, NASA Headquarters Washington, DC United States.

Neukum G., Ivanov B. A. and Hartmann W. K. (2001) Cratering Records in the Inner Solar System in Relation to the Lunar Reference System. In *Chronology and Evolution of Mars* (eds. R. Kallenbach, J. Geiss, and William K. Hartmann). Space Sciences Series of ISSI. Springer Netherlands, Dordrecht. pp. 55–86.

Neukum G., Knig B. and Arkani-Hamed J. (1975) A study of lunar impact crater size-distributions. *The Moon* **12**, 201–229.

Niihara T., Beard S. P., Swindle T. D., Schaffer L. A., Miyamoto H. and Kring D. A. (2019) Evidence for multiple 4.0–3.7 Ga impact events within the Apollo 16 collection. *Meteorit Planet Sci* **54**, 675–698.

Niihara T., Kaiden H., Misawa K. and Sekine T. (2009) U-Pb Isotopic Systematics of Experimentally Shocked Baddeleyite. In id. 1562. 40th Lunar and Planetary Science Conference. Lunar and Planetary Institute, The Woodlands, Texas.

1590 Norman M. D., Bennett V. C. and Ryder G. (2002) Targeting the impactors: siderophile element
1591 signatures of lunar impact melts from Serenitatis. *Earth and Planetary Science Letters*
1592 **202**, 217–228.

1593 Norman M. D., Borg L. E., Nyquist L. E. and Bogard D. D. (2003) Chronology, geochemistry,
1594 and petrology of a ferroan noritic anorthosite clast from Descartes breccia 67215: Clues
1595 to the age, origin, structure, and impact history of the lunar crust. *Meteoritics &*
1596 *Planetary Science* **38**, 645–661.

1597 Norman M. D., Duncan R. A. and Huard J. J. (2006) Identifying impact events within the lunar
1598 cataclysm from 40Ar–39Ar ages and compositions of Apollo 16 impact melt rocks.
1599 *Geochimica et Cosmochimica Acta* **70**, 6032–6049.

1600 Norman M. D., Jourdan F. and Hui S. S. M. (2019) Impact History and Regolith Evolution on
1601 the Moon: Geochemistry and Ages of Glasses from the Apollo 16 Site. *JGR Planets* **124**,
1602 3167–3180.

1603 NRC (2007) *The Scientific Context for Exploration of the Moon*.,

1604 Nyquist L., Bogard D., Yamaguchi A., Shih C.-Y., Karouji Y., Ebihara M., Reese Y., Garrison
1605 D., McKay G. and Takeda H. (2006) Feldspathic clasts in Yamato-86032: Remnants of
1606 the lunar crust with implications for its formation and impact history. *Geochimica et*
1607 *Cosmochimica Acta* **70**, 5990–6015.

1608 Nyquist L. E., Bogard D. D., Shih C.-Y., Greshake A., Stöffler D. and Eugster O. (2001) Ages
1609 and Geologic Histories of Martian Meteorites. In *Chronology and Evolution of Mars*
1610 (eds. R. Kallenbach, J. Geiss, and W. K. Hartmann). Space Sciences Series of ISSI.
1611 Springer Netherlands, Dordrecht. pp. 105–164.

1612 Nyquist L. E. and Shih C. Y. (1992) The isotopic record of lunar volcanism. *Geochimica et*
1613 *Cosmochimica Acta* **56**, 2213–2234.

1614 Nyquist L. E., Wiesmann H., Bansal B., Shih C.-Y., Keith J. E. and Harper C. L. (1995) 146Sm-
1615 142Nd formation interval for the lunar mantle. *Geochimica et Cosmochimica Acta* **59**,
1616 2817–2837.

1617 Ohtake M., Matsunaga T., Haruyama J., Yokota Y., Morota T., Honda C., Ogawa Y., Torii M.,
1618 Miyamoto H., Arai T., Hirata N., Iwasaki A., Nakamura R., Hiroi T., Sugihara T., Takeda
1619 H., Otake H., Pieters C. M., Saiki K., Kitazato K., Abe M., Asada N., Demura H.,
1620 Yamaguchi Y., Sasaki S., Kodama S., Terazono J., Shirao M., Yamaji A., Minami S.,
1621 Akiyama H. and Josset J.-L. (2009) The global distribution of pure anorthosite on the
1622 Moon. *Nature* **461**, 236–240.

1623 Ostertag R. (1983) Shock experiments on feldspar crystals. *J. Geophys. Res.* **88**, B364.

1624 Papanastassiou D. A., Wasserburg G. J. and Burnett D. S. (1970) Rb-Sr ages of lunar rocks from
1625 the sea of tranquillity. *Earth and Planetary Science Letters* **8**, 1–19.

Papike J. J., Burger P. V., Bell A. S. and Shearer C. K. (2018) Mn-Fe Systematics in Martian Olivine: Effect of Mantle Source, Oxygen Fugacity, and Temperature of Crystallization. In Lunar and Planetary Science XLIX. The Woodlands, Texas.

Papike J., Ryder G. and Shearer C. (2006) Lunar Samples. In *Planetary Materials* Reviews in Mineralogy. Mineralogical Society of America. pp. 5–103 to 5–161.

Patchett P. J. and Tatsumoto M. (1981) A routine high-precision method for Lu-Hf isotope geochemistry and chronology. *Contr. Mineral. and Petrol.* **75**, 263–267.

Patchett P. J. and Tatsumoto M. (1980) Lu–Hf total-rock isochron for the eucrite meteorites. *Nature* **288**, 571–574.

Patterson R. V., Frizzell K. R., Kodikara G. R. L., Kopp M., Luchsinger K. M., Madera A., Meier M. L., Paladino T. G., Tai Udovicic C. J., Wroblewski F. B. and Kring D. A. (2022) In situ resource utilization investigations of potential Artemis landing site 105, lunar south pole. In Lunar and Planetary Science LIII. The Woodlands, Texas.

Petro N. E. and Pieters C. M. (2008) The lunar-wide effects of basin ejecta distribution on the early megaregolith. *Meteoritics & Planetary Science* **43**, 1517–1529.

Phinney W. (2015) *Science Training History of the Apollo Astronauts*., NASA.

Pieters C. M., Head J. W., Gaddis L., Jolliff B. and Duke M. (2001) Rock types of South Pole-Aitken basin and extent of basaltic volcanism. *J. Geophys. Res.* **106**, 28001–28022.

Pieters C. M., Staid M. I., Fischer E. M., Tompkins S. and He G. (1994) A Sharper View of Impact Craters from Clementine Data. *Science* **266**, 1844–1848.

Potter R. W. K., Collins G. S., Kiefer W. S., McGovern P. J. and Kring D. A. (2012) Constraining the size of the South Pole-Aitken basin impact. *Icarus* **220**, 730–743.

Prissel T. C. and Prissel K. B. (2021) A lunar sample renaissance. *Nat Commun* **12**, 7053.

Puchtel I. S., Walker R. J., James O. B. and Kring D. A. (2008) Osmium isotope and highly siderophile element systematics of lunar impact melt breccias: implications for the late accretion history of the Moon and Earth. *Geochimica et Cosmochimica Acta* **72**, 3022–3042.

Rankenburg K., Brandon A. D. and Norman M. D. (2007) A Rb–Sr and Sm–Nd isotope geochronology and trace element study of lunar meteorite LaPaz Icefield 02205. *Geochimica et Cosmochimica Acta* **71**, 2120–2135.

Rankenburg K., Brandon A. and Neal C. (2006) Constraints on the formation of the Moon from high-precision and Nd-isotopic measurements of lunar basalts. In Lunar and Planetary Science Conference. Lunar and Planetary Institute, The Woodlands, Texas.

1659 Rapp J. F. and Draper D. S. (2018) Fractional crystallization of the lunar magma ocean:
1660 Updating the dominant paradigm. *Meteorit & Planetary Scien* **53**, 1432–1455.

1661 Rasmussen B., Fletcher I. R. and Muhling J. R. (2008) Pb/Pb geochronology, petrography and
1662 chemistry of Zr-rich accessory minerals (zirconolite, tranquillityite and baddeleyite) in
1663 mare basalt 10047. *Geochimica et Cosmochimica Acta* **72**, 5799–5818.

1664 Reimold W. U. and Stöffler D. (1978) Experimental shock metamorphism of dunite. In Lunar
1665 and Planetary Science Conference IV. The Woodlands, Texas. pp. 2805–2824.

1666 Renne P. R., Balco G., Ludwig K. R., Mundil R. and Min K. (2011) Response to the comment by
1667 W.H. Schwarz et al. on "Joint determination of 40K decay constants and 40Ar∗/40K for
1668 the Fish Canyon sanidine standard, and improved accuracy for 40Ar/39Ar
1669 geochronology" by P.R. Renne et al. (2010). *Geochimica et Cosmochimica Acta* **75**,
1670 5097–5100.

1671 Rubin A. E. (1997) The Hadley Rille enstatite chondrite and its agglutinate-like rim: Impact
1672 melting during accretion to the Moon. *Meteoritics & Planetary Science* **32**, 135–141.

1673 Schaal R. B., Hörz F., Thompson T. D. and Bauer J. F. (1979) Shock metamorphism of
1674 granulated lunar basalt. *Lunar and Planetary Science Conference X*, 2547–2571.

1675 Schaen A. J., Jicha B. R., Hodges K. V., Vermeesch P., Stelten M. E., Mercer C. M., Phillips D.,
1676 Rivera T. A., Jourdan F., Matchan E. L., Hemming S. R., Morgan L. E., Kelley S. P.,
1677 Cassata W. S., Heizler M. T., Vasconcelos P. M., Benowitz J. A., Koppers A. A. P., Mark
1678 D. F., Niespolo E. M., Sprain C. J., Hames W. E., Kuiper K. F., Turrin B. D., Renne P.
1679 R., Ross J., Nomade S., Guillou H., Webb L. E., Cohen B. A., Calvert A. T., Joyce N.,
1680 Ganerød M., Wijbrans J., Ishizuka O., He H., Ramirez A., Pfänder J. A., Lopez-Martínez
1681 M., Qiu H. and Singer B. S. (2020) Interpreting and reporting $^{40}Ar/^{39}Ar$ geochronologic
1682 data. *GSA Bulletin*.

1683 Scherer E., Münker C. and Mezger K. (2001) Calibration of the Lutetium-Hafnium Clock.
1684 *Science* **293**, 683–687.

1685 Schoene B. (2014) U-Th-Pb Geochronology. In *Treatise on Geochemistry* Elsevier. pp. 341–377.

1686 Schoene B., Crowley J. L., Condon D. J., Schmitz M. D. and Bowring S. A. (2006) Reassessing
1687 the uranium decay constants for geochronology using ID-TIMS U–Pb data. *Geochimica*
1688 *et Cosmochimica Acta* **70**, 426–445.

1689 Schultz P. H. and Spudis P. D. (1983) Beginning and end of lunar mare volcanism. *Nature* **302**,
1690 233–236.

1691 Shaulis B. J., Righter M., Lapen T. J., Jolliff B. L. and Irving A. J. (2017) 3.1 Ga crystallization
1692 age for magnesian and ferroan gabbro lithologies in the Northwest Africa 773 clan of
1693 lunar meteorites. *Geochimica et Cosmochimica Acta* **213**, 435–456.

1694 Shearer C., Hess P., Wieczorek M., Pritchard M., Parmentier E., Borg L., Longhi J., Elkins-
1695 Tanton L., Neal C., Antonenko I., Canup R., Halliday A., Grove T., Hager B., Lee D. and
1696 Wiechert U. (2006) Thermal and Magmatic Evolution of the Moon. In *New Views on the*
1697 *Moon* Mineralogical Society of America. pp. 365–518.

1698 Shearer C. K., Elardo S. M., Petro N. E., Borg L. E. and McCubbin F. M. (2015) Origin of the
1699 lunar highlands Mg-suite: An integrated petrology, geochemistry, chronology, and
1700 remote sensing perspective. *American Mineralogist* **100**, 294–325.

1701 Shearer C. K. and Papike J. J. (2005) Early crustal building processes on the moon: Models for
1702 the petrogenesis of the magnesian suite. *Geochimica et Cosmochimica Acta* **69**, 3445–
1703 3461.

1704 Shih C.-Y., Nyquist L. E., Dasch E. J., Bogard D. D., Bansal B. M. and Wiesmann H. (1993)
1705 Ages of pristine noritic clasts from lunar breccias 15445 and 15455. *Geochimica et*
1706 *Cosmochimica Acta* **57**, 915–931.

1707 Shirley M. and Balaban E. (2022) An Overview of Mission Planning for the VIPER Rover.

1708 Silver L. T. (1970) Uranium-Thorium-Lead Isotope Relations in Lunar Materials. *Science* **167**,
1709 468–471.

1710 Snape J. F., Curran N. M., Whitehouse M. J., Nemchin A. A., Joy K. H., Hopkinson T., Anand
1711 M., Bellucci J. J. and Kenny G. G. (2018) Ancient volcanism on the Moon: Insights from
1712 Pb isotopes in the MIL 13317 and Kalahari 009 lunar meteorites. *Earth and Planetary*
1713 *Science Letters* **502**, 84–95.

1714 Söderlund U., Patchett P. J., Vervoort J. D. and Isachsen C. E. (2004) The 176Lu decay constant
1715 determined by Lu–Hf and U–Pb isotope systematics of Precambrian mafic intrusions.
1716 *Earth and Planetary Science Letters* **219**, 311–324.

1717 Spangler R. R., Warasila R. and Delano J. W. (1984) 39AR-40Ar ages for the Apollo 15 green
1718 and yellow volcanic glasses. *J. Geophys. Res.* **89**, B487.

1719 Speyerer E. J. and Robinson M. (2013) Persistently illuminated regions at the lunar poles: Ideal
1720 sites for future exploration. *ICARUS* **222**, 122–136.

1721 Sprung P., Kleine T. and Scherer E. E. (2013) Isotopic evidence for chondritic Lu/Hf and Sm/Nd
1722 of the Moon. *Earth and Planetary Science Letters* **380**, 77–87.

1723 Spudis P. D., Bussey B., Plescia J., Josset J.-L. and Beauvivre S. (2008) Geology of Shackleton
1724 Crater and the south pole of the Moon. *Geophysical Research Letters* **35**.

1725 Spudis P. D. and Davis P. A. (1986) A chemical and petrological model of the lunar crust and
1726 implications for lunar crustal origin. *J. Geophys. Res.* **91**, E84.

Spudis P. D., Hawke B. R. and Lucey P. G. (1988) Materials and formation of the Imbrium Basin. In *A89-10851 01-91* Proceedings of the Lunar and Planetary Science XVIII. Cambridge University Press/Lunar and Planetary Institute, Houston, Texas. pp. 155–168.

Srivastava Y., Basu Sarbadhikari A., Day J. M. D., Yamaguchi A. and Takenouchi A. (2022) A changing thermal regime revealed from shallow to deep basalt source melting in the Moon. *Nat Commun* **13**, 7594.

Staudacher T., Jessberger E., Dominik B., Kirsten T. and Schaefferh O. (1982) Ar-40-Ar-39 ages of rocks and glasses from the Noerdlinger Ries Crater and the temperature history of impact breccias. *Journal of Geophysics* **51**, 1–11.

Steele I. M. and Smith J. V. (1971) Mineralogy of Apollo 15415 "Genesis Rock" : Source of Anorthosite on Moon. *Nature* **234**, 138–140.

Steiger R. H. and Jäger E. (1977) Subcommission on geochronology: Convention on the use of decay constants in geo- and cosmochronology. *Earth and Planetary Science Letters* **36**, 359–362.

Stephan T. and Jessberger E. K. (1992) Isotope systematics and shock-wave metamorphism: III. K-Ar in experimentally and naturally shocked rocks; the Haughton impact structure, Canada. *Geochimica et Cosmochimica Acta* **56**, 1591–1605.

Stöffler D. (1974) Deformation and transformation of rock forming minerals by natural and experimental shock processes. *Fortschr Mineral* **II**, 256–289.

Stöffler D., Bischoff A., Borchardt R., Burghele A., Deutsch A., Jessberger E. K., Ostertag R., Palme H., Spettel B., Reimold W. U., Wacker K. and Wänke H. (1985) Composition and evolution of the lunar crust in the Descartes Highlands, Apollo 16. *J. Geophys. Res.* **90**, C449.

Stöffler D. and Hornemann U. (1972) Quartz and feldspar glasses produced by natural and experimental shock. *Meteoritics* **7**, 371–394.

Stöffler D., Knoll H. D. and Maerz U. (1979) Genetic Classification and Nomenclature of Lunar Highland Rocks Based on the Texture and Geological Setting of Terrestrial Impact Breccias. In Lunar and Planetary Science X. Houston, Texas.

Stöffler D., Knoll H. D., Marvin U. B., Simonds C. H. and Warren P. H. (1980) *Recommended Classification and Nomenclature of Lunar Highland Rocks- a Committee Report*., Lunar and Planetary Institute.

Stöffler D. and Ryder G. (2001) Stratigraphy and Isotope Ages of Lunar Geologic Units: Chronological Standard for the Inner Solar System. In *Chronology and Evolution of Mars* (eds. R. Kallenbach, J. Geiss, and W. K. Hartmann). Space Sciences Series of ISSI. Springer Netherlands, Dordrecht. pp. 9–54.

1762 Stöffler D., Ryder G., Ivanov B. A., Artemieva N. A., Cintala M. J. and Grieve R. A. F. (2006)
1763 Cratering History and Lunar Chronology. In *New Views of the Moon* Reviews in
1764 Mineralogy and Geochemistry. Mineralogical Society of America. pp. 519–596.

1765 Swindle T. D., Isachsen C. E., Weirich J. R. and Kring D. A. (2009) ^{40} Ar- ^{39} Ar ages of H-
1766 chondrite impact melt breccias. *Meteoritics & Planetary Science* **44**, 747–762.

1767 Tai Udovicic C. J., Frizzell K. R., Kodikara G. R. L., Kopp M., Luchsinger K. M., Madera A.,
1768 Meier M. L., Paladino T. G., Patterson R. V., Wroblewski F. B. and Kring D. A. (2022)
1769 Modeling the Effects of Basin Impacts and Ballistic Sedimentation on Ice in Lunar Cold
1770 Traps. In 53rd Lunar and Planetary Science Conference. The Woodlands, TX.

1771 Tatsumoto M. and Rosholt J. N. (1970) Age of the Moon: An Isotopic Study of Uranium-
1772 Thorium-Lead Systematics of Lunar Samples. *Science* **167**, 461–463.

1773 Taylor D. J., McKeegan K. D. and Harrison T. M. (2009) Lu–Hf zircon evidence for rapid lunar
1774 differentiation. *Earth and Planetary Science Letters* **279**, 157–164.

1775 Tera F., Papanastassiou D. A. and Wasserburg G. J. (1974) Isotopic evidence for a terminal lunar
1776 cataclysm. *Earth and Planetary Science Letters* **22**, 1–21.

1777 Touboul M., Kleine T., Bourdon B., Palme H. and Wieler R. (2007) Late formation and
1778 prolonged differentiation of the Moon inferred from W isotopes in lunar metals. *Nature*
1779 **450**, 1206–1209.

1780 Turner G. (1972) 40Ar-39Ar age and cosmic ray irradiation history of the Apollo 15 anorthosite,
1781 15415. *Earth and Planetary Science Letters* **14**, 169–175.

1782 Turner G. (1970) Argon-40/ Argon-39 Dating of Lunar Rock Samples. *Science* **167**, 466–468.

1783 Turner G. and Cadogan P. H. (1975) The history of lunar bombardment inferred from ^{40}Ar-^{39}Ar
1784 dating of highland rocks. *Lunar and Planetary Science Conference Proceedings* **2**, 1509–
1785 1538.

1786 Turner G., Cadogan P. H. and Yonge C. J. (1973) Argon selenochronology. *Lunar and Planetary*
1787 *Science Conference Proceedings* **4**, 1889.

1788 Tye A. R., Fassett C. I., Head J. W., Mazarico E., Basilevsky A. T., Neumann G. A., Smith D. E.
1789 and Zuber M. T. (2015) The age of lunar south circumpolar craters Haworth, Shoemaker,
1790 Faustini, and Shackleton: Implications for regional geology, surface processes, and
1791 volatile sequestration. *Icarus* **255**, 70–77.

1792 Uemoto K., Ohtake M., Haruyama J., Matsunanga T., Yokota Y., Morota T., Nakamura R.,
1793 Yamamoto S. and Iwata T. (2010) Purest anorthosite distribution in the lunar South Pole-
1794 Aitken Basin derived from SELENE Multiband Imager. In 41st Lunar and Planetary
1795 Science Conference. The Woodlands, TX.

1796 Unruh D. M., Stille P., Patchett P. J. and Tatsumoto M. (1984) Lu-Hf and Sm-Nd evolution in
1797 lunar mare basalts. *J. Geophys. Res.* **89**, B459.

1798 Vaughan W. M. and Head J. W. (2014) Impact melt differentiation in the South Pole-Aitken
1799 basin: Some observations and speculations. *Planetary and Space Science* **91**, 101–106.

1800 Villa I. M., De Bièvre P., Holden N. E. and Renne P. R. (2015) IUPAC-IUGS recommendation
1801 on the half life of 87Rb. *Geochimica et Cosmochimica Acta* **164**, 382–385.

1802 Villa I. M., Holden N. E., Possolo A., Ickert R. B., Hibbert D. B. and Renne P. R. (2020)
1803 IUPAC-IUGS recommendation on the half-lives of 147Sm and 146Sm. *Geochimica et*
1804 *Cosmochimica Acta* **285**, 70–77.

1805 Villa I. M., Holden N. E., Possolo A., Ickert R. B., Hibbert D. B., Renne P. R., Bonardi M. L.
1806 and Bièvre P. D. (2022) IUGS–IUPAC recommendations and status reports on the half-
1807 lives of 87Rb, 146Sm, 147Sm, 234U, 235U, and 238U (IUPAC Technical Report). *Pure*
1808 *and Applied Chemistry* **94**, 1085–1092.

1809 Wang S.-J. (2022) First Location And Characterization Of Lunar Highland Clasts In Chang'E-5
1810 Breccias Using TIMA-SEM-EPMA. *At.Spectrosc.* **43**, 351–362.

1811 Warren P. H. and Korotev R. L. (2022) Ground truth constraints and remote sensing of lunar
1812 highland crust composition. *Meteorit & Planetary Scien* **57**, 527–557.

1813 Weirich J. R., Wittmann A., Isachsen C. E., Rumble D., Swindle T. D. and Kring D. A. (2010)
1814 The Ar-Ar age and petrology of Miller Range 05029: Evidence for a large impact in the
1815 very early solar system: Ar-Ar age and petrology of MIL 05029. *Meteoritics & Planetary*
1816 *Science* **45**, 1868–1888.

1817 White L. F., Tait K. T., Kamo S. L., Moser D. E. and Darling J. R. (2020) Highly accurate dating
1818 of micrometre-scale baddeleyite domains through combined focused ion beam extraction
1819 and U–Pb thermal ionization mass spectrometry (FIB-TIMS). *Geochronology* **2**, 177–
1820 186.

1821 Wieczorek M. A. and Zuber M. T. (2001) The composition and origin of the lunar crust:
1822 Constraints from central peaks and crustal thickness modeling. *Geophys. Res. Lett.* **28**,
1823 4023–4026.

1824 Wilhelms D. E., McCauley J. F. and Trask N. J. (1987) *The geologic history of the Moon*.,

1825 Wilshire H. G., Schaber G. G., Silver L. T., Phinney W. C. and Jackson E. D. (1972) Geologic
1826 Setting and Petrology of Apollo 15 Anorthosite (15415). *Geol Soc America Bull* **83**,
1827 1083.

1828 Wilson L. and Head J. W. (1981) Ascent and eruption of basaltic magma on the Earth and Moon.
1829 *J. Geophys. Res.* **86**, 2971–3001.

1830 Wittmann A., Friedrich J. M., Troiano J., Macke R. J., Britt D. T., Swindle T. D., Weirich J. R.,
1831 Rumble D., Lasue J. and Kring D. A. (2011) H/L chondrite LaPaz Icefield 031047 – A
1832 feather of Icarus? *Geochimica et Cosmochimica Acta* **75**, 6140–6159.

1833 Wood J. A. (1970) Petrology of the lunar soil and geophysical implications. *J. Geophys. Res.* **75**,
1834 6497–6513.

1835 Wood J. A., Dickey J. S., Marvin U. B. and Powell B. N. (1970) Lunar Anorthosites. *Science*
1836 **167**, 602–604.

1837 Wu B., Wang Y., Lin T. J., Hu H. and Werner S. C. (2019) Impact cratering in and around the
1838 Orientale Basin: Results from recent high-resolution remote sensing datasets. *Icarus* **333**,
1839 343–355.

1840 Xie M., Liu T. and Xu A. (2020) Ballistic Sedimentation of Impact Crater Ejecta: Implications
1841 for the Provenance of Lunar Samples and the Resurfacing Effect of Ejecta on the Lunar
1842 Surface. *Journal of Geophysical Research: Planets* **125**, e2019JE006113.

1843 Xu Xiaoqing, Hui H., Chen W., Huang S., Neal C. R. and Xu Xisheng (2020) Formation of lunar
1844 highlands anorthosites. *Earth and Planetary Science Letters* **536**, 116138.

1845 Yamamoto S., Nakamura R., Matsunaga T., Ogawa Y., Ishihara Y., Morota T., Hirata N., Ohtake
1846 M., Hiroi T., Yokota Y. and Haruyama J. (2012) Massive layer of pure anorthosite on the
1847 Moon: Pure anorthosite on the Moon. *Geophys. Res. Lett.* **39**, n/a-n/a.

1848 Yamamoto S., Nakamura R., Matsunaga T., Ogawa Y., Ishihara Y., Morota T., Hirata N., Ohtake
1849 M., Hiroi T., Yokota Y. and Haruyama J. (2010) Possible mantle origin of olivine around
1850 lunar impact basins detected by SELENE. *Nature Geosci* **3**, 533–536.

1851 Yokota Y., Matsunaga T., Ohtake M., Haruyama J., Nakamura R., Yamamoto S., Ogawa Y.,
1852 Morota T., Honda C., Saiki K., Nagasawa K., Kitazato K., Sasaki S., Iwasaki A., Demura
1853 H., Hirata N., Hiroi T., Honda R., Iijima Y. and Mizutani H. (2011) Lunar photometric
1854 properties at wavelengths 0.5–1.6 μm acquired by SELENE Spectral Profiler and their
1855 dependency on local albedo and latitudinal zones. *Icarus* **215**, 639–660.

1856 Yue Z., Shi K., Di K., Lin Y. and Gou S. (2022) Progresses and prospects of impact crater
1857 studies. *Sci. China Earth Sci.*

1858 Zellner N. E. B. and Delano J. W. (2015) 40Ar/39Ar ages of lunar impact glasses: Relationships
1859 among Ar diffusivity, chemical composition, shape, and size. *Geochimica et*
1860 *Cosmochimica Acta* **161**, 203–218.

1861 Zellner N. E. B., Delano J. W., Swindle T. D., Barra F., Olsen E. and Whittet D. C. B. (2009)
1862 Apollo 17 regolith, 71501,262: A record of impact events and mare volcanism in lunar
1863 glasses. *Meteoritics & Planetary Science* **44**, 839–851.

Zhang B., Lin Y., Moser D. E., Warren P. H., Hao J., Barker I. R., Shieh S. R. and Bouvier A. (2021) Timing of lunar Mg-suite magmatism constrained by SIMS U-Pb dating of Apollo norite 78238. *Earth and Planetary Science Letters* **569**, 117046.

Zhang J., Yang W., Hu S., Lin Y., Fang G., Li C., Peng W., Zhu S., He Z., Zhou B., Lin H., Yang J., Liu E., Xu Y., Wang J., Yao Z., Zou Y., Yan J. and Ouyang Z. (2015) Volcanic history of the Imbrium basin: A close-up view from the lunar rover Yutu. *Proc. Natl. Acad. Sci. U.S.A.* **112**, 5342–5347.

Zhang W. (2022) In Situ Rb-Sr Dating Of Lunar Meteorites Using Laser Ablation MC-ICP-MS. *At.Spectrosc.* **43**.

Zhu M.-H., Artemieva N., Morbidelli A., Yin Q.-Z., Becker H. and Wünnemann K. (2019) Reconstructing the late-accretion history of the Moon. *Nature* **571**, 226–229.

Zolensky M. E. (1997) Structural water in the Bench Crater chondrite returned from the Moon. *Meteoritics & Planetary Science* **32**, 15–18.

Zolensky M. E., Weisburg M. K. and Buchanan P. C. (1996) Mineralogy of carbonaceous chondrite clasts in HED achondrites and the Moon. *Meteoritics & Planetary Science* **31**, 537.

Zuber M. T., Head J. W., Smith D. E., Neumann G. A., Mazarico E., Torrence M. H., Aharonson O., Tye A. R., Fassett C. I., Rosenburg M. A. and Melosh H. J. (2012) Constraints on the volatile distribution within Shackleton crater at the lunar south pole. *Nature* **486**, 378–381.